Final Draft

of the original manuscript

Santos-Coquillat, A.; Esteban-Lucia, M.; Martinez-Campos, E.; Mohedano, M.; Arrabal, R.; Blawert, C.; Zheludkevich, M.; Matykina, E.:

PEO coatings design for Mg-Ca alloy for cardiovascular stent and bone regeneration applications.

In: Materials Science & Engineering C. Vol. 105 (2019) 110026.
First published online by Elsevier: 29.07.2019

https://dx.doi.org/10.1016/j.msec.2019.110026

PEO coatings design for Mg-Ca alloy for cardiovascular stent and bone regeneration applications

A. Santos-Coquillat[1,2*], M. Esteban-Lucia[1], E. Martinez-Campos[2], M. Mohedano[1], R. Arrabal[1], C. Blawert[4], M. L. Zheludkevich[4], E. Matykina[1,3*]

[1]Departamento de Ingeniería Química y de Materiales, Facultad de Ciencias Químicas, Universidad Complutense, 28040 Madrid, Spain
[2]Tissue Engineering Group, Institute of Biofunctional Studies, Associated Unit to the Institute of Polymer Science and Technology (CSIC), Polymer Functionalization Group, 28040, Madrid, Spain
[3]Institute of Biofunctional Studies, Paseo Juan XXIII, 1, 28040, Madrid, Spain
[4]Institute of Materials Research, Helmholtz-Zentrum Geesthacht, Max-Planck-Straße 1, 21502 Geesthacht, Germany

**Corresponding authors: anamsant@ucm.es; ematykin@ucm.es*

Abstract

Four bioactive PEO (plasma electrolytic oxidation) coatings were generated on Mg0.8Ca alloy using a Ca/P-based electrolyte and adding Si or Fas necessary. Surface characteristics, chemical composition and ion liberation of the coatings were characterized using SEM/EDS (Scanning Electron Microscopy/Energy Dispersive X-ray spectroscopy), X-ray diffraction, optical profilometry and ICP-OES (inductively coupled plasma optical emission spectrometry). Direct biocompatibility studies were performed by seeding premyoblastic, endothelial and preosteoblastic cell lines over the coatings. Biocompatibility of the coatings was also evaluated with respect to murine endothelial, preosteoblastic, preosteoclastic and premyoblastic cell cultures using extracts obtained by the immersion degradation of the PEO-coated specimens. The coatings reduced the degradation of magnesium alloy and released Mg Ca, P, Si and F. Of all the studied compositions, the Si-containing PEO coating exhibited the optimal characteristics for use in all potential applications, including bone regeneration and cardiovascular applications. Coatings with high F content negatively influenced the endothelial cells. RAW 264.7, MC3T3 and co-culture differentiation studies using extracts of PEO coated Mg0.8Ca demonstrated improved osteoclastogenesis and osteoblastogenesis processes compared to bare alloy.

Keywords

Magnesium; Biodegradable implants; Coating; Extract; Osteoblast; Osteoclast; Co-culture

1. Introduction

Mg alloys are being actively explored as highly biocompatible materials for bone reconstruction plates and cardiovascular stents[1, 2]. The advantages of using Mg are numerous: no need of second surgery for removal of the implant and shorter degradation periods and greater load-bearing capacity compared with polymeric alternatives. Mg-based biodegradable materials are useful for bone-growing situations, such as developmental processes in children, including paediatric treatment of fractures or congenital defects. Evaluation of Mg alloy implants in musculoskeletal applications produces an interesting bone tissue response that has been overshadowed by their *in vivo* corrosion behaviour[3, 4]: H_2 gas formation as a degradation product can interfere with the healing process, and excessive mass loss can affect mechanical stability of bone reconstruction plates[5]. As a consequence, only a few commercial Mg-based implants are available (e.g. MAGNEZIX®, Magmaris by BIOTRONIK) moreover some commercial Mg alloys (e.g. Mg-Zn-RE) have also been clinically approved for biomedical use[6].

The degradation rate of Mg can be controlled via adequate alloy design: a large variety of alloying elements has been studied in order to improve Mg implants behaviour for biomedical applications [7]. These elements ought to provide mechanical strengthening and/or improve the degradation rate without causing cytotoxicity. For example, Ca and Zn are highly biocompatible and improve the mechanical properties (ductility and age hardening) while being relatively inert corrosion-wise if used in concentrations below 1 wt.%, and Ag improves tensile strength providing an additional antibacterial effect[8].

As an additional strategy, surface treatments such as chemical conversion coatings[9], anodizing techniques[10], ion implantation[11], sol-gel coatings[12], plasma spraying[13]and other modifications such as hydroxyapatite[14], bioactive glasses, bioceramics[15], among others[16], can further reduce the degradation rate of Mg alloys. Plasma electrolytic oxidation (PEO), employed in this study, is an advanced anodizing technique that generates ceramic-like coatings with a composition, microstructure, porosity, and roughness easily controlled by the electrical parameters of the process and the composition of the electrolyte. Moreover, PEO coatings also enable excellent control of magnesium corrosion rate [10, 17, 18], besides of reducing production costs in comparison to other surface treatments. As a result, a thick and stable covering is achieved over Mg implant, a feature that can upregulate cell response.

It is well known that topographic modification of the PEO coating surface can increase bone cell activity [19]. On the other hand, the electrolyte design is a key to incorporation of bioactive elements into the coating and has proven to modulate the biological response of bone cell lineages, such as bone-forming cells (osteoblasts) and bone resorbing cells (osteoclasts). In this sense, a significant effort is needed to create a real bioceramic covering able to positively interact with bone cell populations and fulfil medical requirements.

Phosphate incorporation into the electrolyte favours the integration of various compounds into the coating, such as magnesium phosphate or magnesium fluoride, improving corrosion resistance[20]. Zeng*et al.* produced a very thin PEO coating using a phosphorous source in the electrolyte composition and employed a PLA(polylactic acid) coating post-treatment strategy[21]. The biological importance of incorporating Si into PEO coatings has been demonstrated using MG63 osteoblasts evaluating cell adhesion, proliferation and differentiation using Mg-Ca (1 wt.%) alloy[22]. Si is a key component in the bone metabolism, the presence of Si in contact with osteoblasts promotes the synthesis of collagen and matrix

mineralization [23, 24]. A study by Zhang *et al.* [25] using AZ31B alloy evidenced the incorporation of species of Ca, P and Si by PEO technique and the formation of phases (Mg_2SiO_4) that favoured not only adhesion and proliferation of BMSC (Bone Marrow Stromal Cell) but also the osteoblastogenesis. Furthermore, Si incorporation into the electrolyte showed an increased Ca/P ratio in the coating as the Ca incorporation was promoted in PEO on titanium [26].

Moreover, the release of integrated species from the coating to the culture medium can also affect bone cell lineages, both directly over the coating or in the near implant microenvironment. The presence of Mg in culture medium has demonstrated an augmented expression of alkaline phosphatase activity, an early osteoblastic marker of bone matrix synthesis [27]. On the other hand, osteoclasts are known to be sensible to Mg [27], Si [28] and other elements. Additionally, the formation of compounds such as HA, FA or other apatites will promote the resorption process favouring a balanced homeostasis in the implant area. A previous work of the authors on PEO of Mg0.8Ca alloy proved that the incorporation of Ca, P and F into the electrolyte promoted the formation of fluorapatite (FA) and hydroxyapatite (HA) in the coating while increasing the coating thickness and favouring both corrosion resistance and human osteoblast adhesion and proliferation processes[10].

In this sense, *in vivo* successful bone remodelling is promoted by a proper environment able to maintain the communication between bone cell lineages, and therefore, internal bone tissue homeostasis. Thus, accurate *in vitro* models are required to emulate the complexity of *in vivo* conditions. In this context, co-cultures [29, 30] of both cell types have been developed to assess the possible implantation success of the biodegradable materials. In the past years, as a consequence of the development of magnesium alloys and PEO-coated magnesium as biodegradable implants, several *in vivo* studies [31-40] have been conducted. Although many

in vivo studies have been performed during last decades, several problems associated with degradation behaviour were encountered, such as generation of hydrogen gas bubbles and local alkalization. Because of that, new coating designs are needed to fulfil these requirements.

The aim of this study is to generate graded compositions of PEO coatings on Mg0.8Ca alloy using electrolytes containing bioactive elements (Ca, P, F and Si) to evaluate the liberation of bioactive elements from the coatings and the effect of thereof on biological performance of the obtained materials by direct studies and extracts incubation using premyoblast, endothelial, osteoblast and osteoclast cell models.

2. Experimental procedure

2.1 Materials

Mg 0.8 wt. % Ca alloy (mass fraction: 0.61% Ca, 0.003% Fe, 0.0021% Cu, 0.0009% Ni, 0.023% Si %, 0.02% Al, 0.006% Zn, 0.05% Mn, 0.000039% Be and Mg balance) was selected as substrate. All the samples were ground successively with SiC papers to P1200 grit size and cleaned with deionized water and isopropanol before the PEO treatment.

2.2. PEO treatment

The electrolytes were designed adding NaF or Na_2SiO_3 into the base Ca-P-containing electrolyte as necessary, adjusting the concentrations in preliminary trials in order to maintain the electrolyte conductivity suitable for sustainable microdischarges (within 14-30 $mScm^{-1}$) and achieve uniform coatings. The final compositions of the studied electrolytes are given in Table 1. PEO treatments were carried out for 300 s as described before[10]. After PEO, the specimens were rinsed in deionized water and dried in warm air.

2.3. Surface characterization

Plan views and cross-sections of the coatings were examined by scanning electron microscopy (SEM) using a JEOL JSM6400 instrument equipped with Oxford Link energy dispersive X-ray (EDS) microanalysis spectrometer. Metallographic preparation of the cross-sections was carried out by grinding through successive grades (P600-P1200) of SiC paper and final polishing with 0.1 μm diamond paste. X-ray diffraction (XRD) patterns were obtained using a Philips X'Pert diffractometer (CuKα = 0.154056 nm, 0.01º /second scanning speed, 2□ range: 10 to 90º) and phases were identified with the PANalytical's X'PertHighScore software and the ICDD PDF4+ database. Roughness parameters (R_a and R_z) were obtained using a Surtronic 25 roughness tester (Taylor Hobson) and Talyprofile software. The presented values are an average of 3 measurements performed over a length of 2.8 mm. A focus-variation optical 3D profilometer (InfiniteFocus SL, ALICONA) was used to evaluate R_a (arithmetic mean deviation of the assessed profile), S_a (arithmetical mean height of the area), S_v (maximum pit S_{10z} (ten-point height) roughness parameters.Coating thickness was measured using a Fischer ISOSCOPE FMP10 portable eddy current meter, obtaining an average of ten measurements, and later confirmed with cross-sectional SEM. Vickers microhardness was measured on coating cross-sections using AKASHI MVK-E3.The pore population density and pore size of the coatings were estimated using ImageJ software. Image analysis of the coating surface was carried out using three SEM micrographs taken at arbitrarily locations.

2.4. Ion release analysis

Immersion tests were performed at (37±0.5) ºC using specimens with a total exposed area of 3.7 cm^2 placed in tightly sealed containers with 20 mL of 0.9% NaCl solution. Mg, Si, P and Ca ions release was analysed after 5 days of immersion by ICP-OES with a Perkin-Elmer 3300 DV instrument, operating at RF power of 1.3 kW, with a plasma flow of 1 L^{-1}, sample flow rate of 0.8 mL min^{-1} and argon (plasma maintaining carrier gas) flow of 0.8 L min^{-1}[41]. The results are cited as an average of three replica measurements. F^- release was measured at 24

hours and 5 days of immersion in 20 mL of 0.9% NaCl solution (total exposed area of 3.7 cm^2) by ISE (Ion Selective Electrode) following the procedure described elsewhere [41]. Two specimens for each type of material were used for reproducibility. The pH measurements of the cell culture were carried out using a Crison 5028 microelectrode and a Crison pH Basic 20 instrument.

2.5 Cell culture

C2C12-GFP (ATCC® CRL-1772™) mouse premyoblast cell line and C166-GFPendothelial cell line (ATCC® CRL-2583™) were incubated at 37 °C with 5% CO_2 with complete Dulbecco's MEM (D6429, Sigma-Aldrich) supplemented with 10% fetal bovine serum (FBS, Hyclone®, Thermo Scientific) plus antibiotics (100 U/mL penicillin and 100 μg/mL streptomycin sulphate, Sigma-Aldrich). Green Fluorescent Protein (GFP) was expressed due to previous lentivirus infection of C2C12-GFP cell line. C166-GFP cell line requires the addition G-418 antibiotic at a final concentration of 0.2 mg/mL for the maintenance of the fluorescence. MC3T3-E1 cell line (ATCC® CRL-2593™) is a mouse preosteoblastic cell line. Cells were cultured in complete α-MEM (A10490, Gibco) without ascorbic acid. RAW 264.7 cell line (ATCC® TIB-71™) was used as an osteoclast differentiation model from a mouse macrophage population as described before[42]. RAW 264.7 cells are maintained in an undifferentiated state by culture in and the medium, complete DMEM, was changed every three days.

2.6 NaF cytotoxicity

C166-GFP, C2C12-GFP and MC3T3 cell lines were incubated for 24 hours with known concentrations of NaF. Cells were seeded with a density of 1.5×10^4 cells/cm^2 at a 24 well plate. Different concentrations of NaF (mM): 0.5, 1, 1.75, 2.5, 5 and 7.5 were evaluated.

Metabolic activity was measured in NaF treated at 24 h. Alamar Blue assay (Biosource) was performed as previously described[43], with this technique an estimation of cytocompatiblity and viability can be obtained. Each condition was analyzed in triplicate.

2.7 Direct studies

For *in vitro* studies samples were cut into 1 cm^2. In order to sterilize the selected materials, samples were left overnight with absolute ethanol and 45 min of UV exposition for each side of the bare/substrate material, titanium CP (used as positive control) and the PEO coated samples. C166-GFP and C2C12-GFP were seeded over the materials at a density of 3×10^4 cell per $cm^2$for 30 min. Both cell lines were evaluated during the days by fluorescence microscopy (FITC filter λex/λem = 490/525 nm) with inverted fluorescence microscope (Olympus IX51), this was possible due to its fluorescence. MC3T3 were seeded over the samples at a density of 3×10^4 cells per cm^2. For the evaluation of this cell line an Actin and Hoescht staining as described before[42] was performed after 5 days of culture over the materials. Complete medium was changed every day to avoid alkalization in all the experiments. After 5 days growing, premyoblastic cells were fixed and dehydrated with several ethanol gradients of increased concentrations and dried in a chamber with silica gel. SEM images of C2C12-GFP were taken at 20 kV.

2.8 Studies with extracts

Mg0.8Ca alloy and PEO coated samples were maintained in complete DMEM (FBS and P/S) during 5 days with an immersion ratio[44, 45] of 1.25 mL per cm^2 and simulated *in vitro* conditions (37ºC, 95% relative humidity and 5% CO_2). The extract media obtained in this manner were used for the following *in vitro* studies.

2.8.1 Cytocompatibility

For cytocompatibility studies ratios of 1:2 and 1:10 (Extract: DMEM) were selected and evaluated with C2C12-GFP and C166-GFP. Cells were plated at 1.5×10^4 cells/cm^2 and cultured for 5 days. Alamar Blue measurements were done at day 5 as described above.

2.8.2 Cell differentiation

For differentiation studies a 1:4 extraction medium; α-MEM or DMEM ratio was selected based on previous bibliography[29] with these two differentiation murine models. For extract studies MC3T3 cells were plated with a seeding concentration of 1.5×10^4 cells/cm^2 at 24 well plates. Cells were cultured for 7 days in 1:4 extract, changed to differentiation medium and left incubating for another 7 days. Differentiation medium consisted in completed maintenance medium with 50 μg/mL ascorbic acid, 10 nM dexamethasone and 10 mM β-glycerolphosphate. Complete differentiation medium was changed every 2 or 3 days. For extract incubation, RAW 264.7 cells were seeded in TCP (24 well plates, Corning Costar) at 1.5×10^4 cells per cm^2 and supplemented with 50 ng/mL of recombinant RANKL (Receptor Activator of NFκb Ligand, PeproTech). At day 3 extract medium with RANKL was changed with completed differentiation fresh medium (complete DMEM with RANKL).

In co-culture studies, MC3T3 cells were plated at 1×10^4 cells/cm^2 at 24 well plates and allowed to grow for 24 hours in complete α-MEM medium. After this time, RAW 264.7 cells were seeded over the preosteoblasts at a final concentration of 1.5×10^4 cells per cm^2 in 1:4 extract medium. RANKL was added when the macrophages where plated and refreshed when the extract medium was changed at day 3. The cells were co-cultured for 5 days (D1 starting after RAW 264.7 seeding). Actin and Hoechst staining as described elsewhere [42] was performed at endpoint.

2.8.3. Collagen secretion (Sirius Red Staining)

Collagen secretion of the MC3T3 cells cultured in the extract medium was evaluated by Sirius Red staining. After 14 days, cells were fixed and stained as described before[41]. Sirius Red stained samples were measured with a Microplate Reader per triplicate.

2.8.4. Mineralization (Alizarin Red)

Calcium deposits in the cells were confirmed by staining with Alizarin Red-S (AR-S, Sigma). After 14 days, cells were fixed with 4% paraformaldehyde (PFA) solution for 15 min, washed twice with deionized water and incubated with 40 mM AR-S at pH 4.1 for 30 min at room temperature. Then, after washing 3 times with deionized water to remove free Ca ions, the stained cultures were photographed with an inverted optical microscope (Olympus IX51).

2.8.5. Osteoclastogenesis (TRAP staining)

TRAP (Tartrate Resistant Acid Phosphatase) staining was performed using a commercial kit by the manufacture instructions (Sigma-Aldrich). Cells were incubated in a solution of Naphthol AS-BI phosphoric acid and Fast Garnet GBC. This kit is used to demonstrate tartrate resistant acid phosphatase (TRAP), an enzyme that it is expressed during osteoclastogenesis.

2.8.6. Statistical analysis

Statistical analysis (mean ± standard deviation) of AlamarBlue and Sirius red was performed using a 95% confidence interval ($p<0.05$) and one-way ANOVA followed by Tukey's post-hoc test with Graph Pad Prism8 software. Significant differences stand for *($p\leq0.033$), **($p \leq0.002$), ***($p \leq0.001$).

3. Results

3.1. Electrical response of PEO treatment

Figure 1 shows the evolution of rms voltage during PEO treatment in PEO-B, PEO-4F, PEO-8F and PEO-9Si electrolytes (Table 1). During the applied voltage ramp a linear voltage increase is observed; in the case of PEO-8F the first inflexion point occurs at 45 s associated with the initiation of plasma microdischarges on the surface of the material. The second change of slope occurs when the microdischarges uniformly cover the surface; the voltage slope decreases significantly and the coating growth is limited by the set current limit. When coating

impedance increases up to a certain point, a constant V_{rms} corresponding to the set pulse amplitudes is reached, and, consequently, the current drops (not shown). By the end of the treatment PEO-B and PEO-9Si present a constant V_{rms} of ~300 V whereas for PEO-8F and PEO-4F electrolytes the final formation voltage is ~240 and ~260 V, respectively. Further, a change of slope at 200 s after a relatively flat region is present in both PEO-4F and PEO-8F electrolytes. Visual examination of the discharges was not possible because of insolubility of CaO and the resulting opacity of the electrolytes with suspended particles.

3.2. Coating characterization

The surface morphologies and cross sections of the formed PEO coatings with indication of their respective surface area and local area EDS analysis are presented in Figure 2 (Table 2). PEO-B exhibited the lowest thickness (~6 μm) with a submicrometric size porosity and a reduced roughness (R_a ~0.7 μm) (Figure 2, Table 3).

The addition of Si into the electrolyte doubled the thickness of the coating (~13 μm). PEO-9Si surface morphology revealed a homogeneous pore size and bulgy areas between the pores as depicted in Figure 2, resembling bone structure. Cross-sectional examination indicated a greater compactness and uniformity of PEO-9Si in comparison to the other coatings. R_a (0.84 μm) was similar to PEO-B.

F-containing coatings were thicker (~48 μm), however some characteristics differed between them. PEO-4F had a two-layer morphology comprising an outer layer with large sparse cavities and an inner layer with numerous small pores (Figure 2). Formation of large voids is a result of intense microdischarges and copious gas liberation, which are manifested by significant voltage oscillation in case of PEO-4F (Figure 1). PEO-8F coating, on the other hand, was more compact and homogeneous without differentiated layers visible at this magnification. Transversal

porosity was evaluated for both coatings (Table 3) and yielded the maximum pore size of 115 μm^2 and 30 μm^2 for PEO-4F and PEO-8F, respectively.

Surface morphology of PEO-4F and PEO-8F comprised large surface cavities of complex shape rather than defined pores, which introduced great artifacts into the estimation of surface porosity by image analysis. Surface microcracks related to thermal stresses from a quick cooling process were also observed in PEO-8F. The roughness values (R_a) were almost 5-6 fold higher (4.3 µm and 3.6 µm) than for PEO-B and PEO-9Si coatings (Table 3).

A semiquantitative analysis of the elemental composition of the coatings was performed by EDS (Table 2). The composition of the electrolytes determined the composition of the PEO coatings. For instance, F and Si were readily incorporated into the PEO-F and PEO-Si coatings, respectively. Elevated Ca/P ratios were observed for F-containing electrolytes (Figure 2, locations 3 and 6), with this ratio being greater in the outer part of the PEO-4F and PEO-8F coatings (1.3 and 1.5, respectively). A compositional difference was detected by local area analysis between the inner and the outer regions of the coatings, showing a much higher Ca/P ratio in the outer part. The opposite scenario appeared in PEO-9Si where the local area analysis in the inner part presented very little presence of P and a greater content of Ca (2.21%) than in the surface area or outer part analysis with a Ca/P ratio of 0.45 and 0.16. Si appeared in a higher amount in the outer region of the coating, reaching up to 12%. Increased F content was observed in the inner parts of PEO-4F and PEO-8F, reaching up to ~24% and ~39%, respectively. NaF addition into the electrolyte composition resulted in increased thickness and roughness of the coatings, in agreement with previous work [10]. Furthermore, the increase of NaF concentration (from 4 g L^{-1} to 8 gL^{-1}) resulted in a more compact coating with lesser transversal porosity and two times greater microhardness (Table 3). Also, PEO-8F coating was ~1.5 times harder than PEO-9Si, demonstrating that both the composition and compactness of the coatings affect the

values of microhardness. Lower hardness of PEO-9Si compared to PEO-8F can be related to the presence of micron-size porosity discernible in the coating cross-section (Figure 2). If the indenter hits some of these underlying pores, it yields lower hardness values. PEO-8F, being much thicker and featuring greater stretches of relatively dense, pore-free zones, can better accommodate the indenter.

Figure 3A displays the X-ray diffraction patterns of the formed PEO coatings. XRD examination depicted high intensity peaks of Mg proceeding from the base material. All the coatings consisted of a MgO matrix and presence of amorphous material in accordance with a peak broadening between 25-35º 2θ. In PEO-B hydroxyapatite (HA; $Ca_5(PO_4)_3(OH)$), $CaMg_2$and $Ca(OH)_2$ were formed.PEO-9Si presented peaks for HA (with higher intensity than in PEO-B), Mg_2SiO_4 (forsterite), $Ca(OH)_2$ and Ca_3 $(PO_4)_2$. On the other hand, fluoride-containing electrolytes promoted the formation of MgF_2, Mg fluorophosphate and $Ca_5(PO_4)_3F$ (fluorapatite; FA). CaF_2 and $Ca(OH)_2$ were also formed in PEO-8F.

3.3. Ion release

Mg, Ca, P, Si and F ion liberation from the coatings was evaluated by ICP-OES and ISE after their immersion in 0.9% wt.% NaCl at 37ºC during 5 days (Table 4). Additionally, Mg and Ca liberation from non-coated Mg0.8Ca substrate was measured. All these species participate in cell metabolism, e.g. Ca and P are important for the formation of HA during bone matrix mineralization and F is known for its antibacterial properties[46].The following findings of the ion liberation from the studied PEO coatings showed that the ion lixiviation was determined by the element content in the coating, the coating thickness and the structure of the compounds incorporated into the ceramic layer. Mg released from the uncoated substrate (65 to 417 μg $cm^{-2}d^{-1}$) proceeded from corrosion process; the elevated variation in this value was due to

development of pits in some of the specimens (Supplementary Figure 1). Mg release from the PEO-B coated substrate was reduced by about 5 times (46 μg $cm^{-2}d^{-1}$). On the other hand, the Mg release from thicker coatings (PEO-4F and PEO-8F) containing MgF_2 and $Mg_2(PO_4)F$ was greater than from the non-coated substrate. Ca and P ion liberation from the coatings that contained F was also increased in compared with PEO-B coating. There were no significant differences between the ion release from PEO-4F and PEO-8F. F^- liberation was determined at two time points, 1 and 5 days (Table 5), using fluoride ion selective electrode. An evident decrease in the free F^- with time was observed. The greater liberation in the first day from PEO-8F coating is consistent with the higher fluoride content in the coating, compared with PEO-4F.

3.4. Biological evaluation

3.4.1. Cell culture over the materials

In order to evaluate biological behaviour, cell cultures were seeded over the following specimens: non-coated Mg0.8Ca and commercially pure titanium as control materials; PEO-B, PEO-4F, PEO-8F and PEO-9Si coatings. Three different cell types were used: endothelial (C166-GFP), premyoblastic (C2C12-GFP) and preosteoblastic (MC3T3) murine cell lines. This selection covers a wide range of cell response as cell lineages react differently to the same topographic and bioactive characteristics.

Figure 4 depicts fluorescence micrographs of the three cell types growing on the materials at day 5. C166-GFP and C2C12-GFP were evaluated daily thanks to their fluorescence; both cell types were unable to grow and proliferate over Mg0.8Ca. On the contrary, they formed a dense monolayer over Ti CP (the positive control), as expected. The premyoblastic cell line, C2C12-GFP, showed a good performance in all the coatings with a greater result in terms of monolayer formation in PEO-9Si. On the other hand, C166-GFP cells exhibited a differential behaviour over the PEO-coated materials. In PEO-4F these cells were not able to form a monolayer and

in PEO-B the formed monolayer was unorganized. In contrast, in PEO-9Si the cells were able to organize themselves following the surface topography. Related to early adhesion times of C2C12-GFP and C166-GFP (24 h) Supplementary Figure 2 shows that more cells were able to adhere and survive over the bare alloy for both cell lines. A monolayer was already formed in Ti CP after this short time.

An Actin and Hoechst staining was performed in order to assess the cellular performance of MC3T3 cells over the surfaces. These cells successfully formed a monolayer in Ti CP, and, unlike endothelial and premyoblastic cells, a larger number of cells were able to survive in Mg0.8Ca. PEO-4F and PEO-8F coatings did not promote the monolayer formation, although higher number of cells could be seen in PEO-8F, indicating that the decreased long-term liberation of fluoride from these coatings, compared with PEO-4F,determines this outcome, as predicted by the preliminary NaF cytotoxicity study (Supplementary Figure 3).The reduced performance of preosteoblasts on fluoride-containing coatings can be also related to the greater roughness of both coatings with R_a values around 4 µm (Table 3). The latter fact contrasts with the good performance of the preosteoblastic cells in terms of monolayer formation in PEO-B and PEO-9Si with R_a values less than 1 µm (Table 3), suggesting that a less uneven topography is preferential for the ability to form a monolayer. Moreover, PEO-9Si demonstrated an improved preosteoblast growth, with a denser monolayer and higher number of stained nuclei, in comparison with Ti CP control. PEO-9Si was the only coating with a regular surface porosity (Figure 2) resembling that of the trabecular bone.

Lastly, SEM examination of the preomyoblastic cell line (C2C12-GFP) after 5 days of growth was carried out in order to see the interaction with the surface of the PEO coatings and the monolayer disposition (Figure 5). A well-formed monolayer was revealed in all the PEO-coated surfaces (right row, Figure 5). Higher magnification micrographs of selected areas (left row,

Figure 5) disclosed the individual cell morphology and cell interactions with the surface. The premyoblastic cells appeared to be growing similarly in PEO-4F and PEO-8F coatings, "hovering" over the uneven topography. The cell morphology was more elongated in PEO-B and PEO-9Si and much closer adhered to the surface, as the coatings are less rough. In PEO-B, the cracking of the surface (as a result of the undercoating corrosion) was visible; on the contrary, PEO-9Si surface appearance post-immersion practically did not alter compared with the as-received surface state (Figure 2). Moreover, the cells appeared to be interacting with the surface pores by means of filopodia and lamellipodia.

3.4.2. Extract preparation

In order to evaluate the cellular implication of the elements, incubation of the PEO-coated and non-coated substrate in complete DMEM was performed during 5 days simulating cell culture conditions (37ºC, 5% CO_2 and 95% humidity). The obtained extracts were subsequently used for differentiation and co-culture cell work. Extracts present simplified conditions, since there is no a gradient of pH and element concentration with time, which ensure greater reproducibility of the cell work.

After the immersion in this medium, the samples were assessed by optical profilometry (Figure 6), obtaining roughness characteristics of the surfaces. The non-coated substrate presented a layer consisting of corrosion products ($Mg(OH)_2$ typically) and deposits from the enriched DMEM solution (these could include both inorganic and organic components, e.g. FBS proteins). Therefore, the R_a and S_a values of the surface increased to ~1.3 and ~2.3 µm (Figure 6). Some pitting as deep as 40 µm, formed due to the corrosion process, was present (Figure 6, centre row 2D simulation). PEO-B disclosed a R_a value of 0.5 µm (slightly smaller than before the immersion) and a S_v of 28.5µm corresponding to the deep pit. PEO-4F and PEO-8F retained the high roughness values similar to those measured before the incubation, with a slight increase

in R_a for PEO-4F, as some areas revealed detachment and/or loosening of the top part of the coating. In fact, the 3D rendering of the coating surface reveals bold patches that are up to 29.5 µm deep (S_v), which correlates with the thickness of the outer coating layer as observed in Figure 2. The PEO-8F and PEO-9Si coatings which reveal a more homogeneous surface and maintain the as-received surface characteristics can be expected to offer greater corrosion protection.

XRD examination of the coatings after immersion (Figure 3B) showed similar patterns in comparison to those for the as received coatings. Less amorphous material was present after the exposure to DMEM, Mg and MgO peaks intensity in all the coatings was lower, which can be associated with corrosion process. The intensity of the peaks corresponding to HA in PEO-B and PEO-9Si coatings has also decreased; similarly, the intensity of FA, Mg_2PO_4F and MgF_2 peaks decreased in PEO-4F and PEO-8F.

3.4.3. Extracts Cytocompatibility

A preliminary analysis of cell response was carried out using a range of NaF concentrations, as liberated F^- can be a toxic stimulus to cell cultures (Supplementary Figure 3). Endothelial cells turned out to be the more sensible ones as it has previously been described [47], with a tolerance limit ≤1.0-1.75 mM, followed by the preosteoblastic cells. Premyoblastic cells showed the most robust behaviour of all the cell lines, starting to be affected at a concentration >2.5 mM NaF.

The extracts obtained as described in the experimental section were evaluated in terms of cell growth and metabolic activity levels. For this evaluation two ratios were selected, representing highly unfavourable and highly favourable conditions, respectively: a concentrated extract (1:2) and a highly diluted extract (1:10), the latter simulating the physiological state with a pH≈7.4, i.e. close to that of the matrix DMEM non-modified with coating-derived ions. Figure 7A presents micrographs of C166-GFP and C2C12-GFP after 5 days cultured with the 1:2 extract.

As expected with Mg0.8Ca, cells were highly affected and were not able to proliferate in none of the two cell lines. On the other hand, F-free PEO-9Si coating exhibited the best biological performance of all the PEO coatings with dense monolayer formation (even despite the pH≈8.0), and the higher metabolic activity levels in both endothelial and preomyoblastic cells. An important difference in the effect of PEO-8F extract on the behaviour of C166-GFP cells and C2C12-GFP cells, depicted in Figure 7B, is related to the fluoride cytotoxicity observed for C166-GFP (Supplementary Figure 3), as PEO-8F has the highest release of F^- at short times. The F^- concentration in the PEO-8F 1:2 diluted extract can be estimated as ~44 ppm or ~2.3. mM, which is above the F^- tolerance limit determined initially.

Figure 8A shows that in 1:10 extracts a monolayer was formed after 5 days of the incubation time for both cell lines. This is associated with the absence of alkalinisation of the culture medium and, in case of F-containing coatings, the fact that F^- concentration was ≤8.8 ppm or ≤0.46 mM, i.e. well within the tolerance limit. Moreover, under these dilute conditions a clear increase in metabolic activity can be detected (Fig. 8B), especially with PEO-8F and PEO-9Si extracts in both cell lines, which can promote metabolic intracellular pathways. In regards to coating-derived ion concentration effect on metabolic activity, the Mg0.8Ca extract containing~81 ppm of Mg and ~2 ppm of Ca exhibited the same response as matrix DMEM (on TCP control). PEO-4F and PEO-8F extracts contained ~1.5 times greater amount of Mg and 2-3 times greater amount of Ca than the Mg0.8Ca and showed a superior performance. Finally, the PEO-9Si extract, containing ~26 ppm of Mg, ~0.4 ppm each of Ca and P and ~0.8 ppm of Si, exhibited the greatest of all metabolic activity.

3.4.4. Differentiation evaluation in extracts

In order to predict the *in vivo* bone cell behaviour in presence of the studied materials, MC3T3 preosteoblasts and RAW 264.7 osteoclast precursor were selected and differentiation processes

evaluated under the incubation with an extract 1:4, the dilution reported in other works on co-cultures[29]. This dilution ensures approximately the same coating-derived ion concentration in the media as in the ion liberation experiments (Tables 4 and 5).

The preosteoblastic cell line was incubated during 7 days. At that time point, an AlamarBlue was performed as well as collagen secretion quantification (Supplementary Figure 4). The culture was also left for another 7 days with differentiation medium (14 days end point), at which point collagen secretion (Figure 9) and calcium deposits formation indicating mineralization were evaluated (Figure 10). No significant differences were found between the metabolic activity of the substrate alloy and the PEO coatings (PEO-4F, PEO-8F and PEO-9Si) extracts, only a significant reduced level was found for PEO-B, showing that at 1:4 dilution the pH alkalinisation was not affecting the cells. Although, pH measurements of the extracts in day 7 evidenced a higher alkalinisation in Mg0.8Ca extract with a pH of 8.6 versus pH 8 in all the other samples. Related to the differentiation markers, all the conditions showed collagen secretion as revealed by Sirius Red staining with a nodular disposition at 14 days, especially evident in case of PEO-9Si extract (Figure 9C, detailed micrograph). Only PEO-B showed a significant reduction of collagen secretion at 7 and 14 days. In addition, PEO-9Si extract presented calcium deposits with red rounded areas (Alizarin Red staining) at day 7 and 14 (Figure 10), although all the conditions were positive for the staining, indicating that a mineralized matrix is present in all cases.

The importance of the osteoclastogenesis process in biodegradable materials performance has not yet been fully addressed. One of the main applications of Mg implants is bone regeneration. In this sense, the importance of a well-functioning homeostasis process in the implant microenvironment has to be highlighted. Therefore, macrophages were incubated with the samples extracts and RANKL, the key in the osteoclastic differentiation process

mechanism[48]. Figure 11 presents a TRAP staining of the formed osteoclasts under these conditions after 5 days of incubation (first 3 days with extracts incubation and further 2 days with fresh medium without extract and refreshed RANKL). In Mg0.8Ca extract, the phenotype could not be rescued and only small osteoclasts were formed after 5 days. On the other hand, big osteoclasts were formed in all PEO coatings extracts incubation. PEO-B and PEO-4F presented also a high number of mononucleated cells and less osteoclasts distribution per area. Finally, the osteoclasts were most abundant in PEO-8F and PEO-9Si.

3.4.5. Co-cultures of Osteoblasts and Osteoclasts

A co-culture with RAW 264.7 macrophages and MC3T3 preosteoblasts was seeded with the extract 1:4 for 5 days. Bone regeneration is a well-regulated process where osteoblasts (bone matrix secretors) and osteoclasts (bone resorbing agents) communicate with each other and finally promote tissue healing. Because of that, the analysis of the whole system in a controlled environment can provide clues for prediction of future *in vivo* results. As with osteoclasts study, the medium was changed at day 3 without extract and RANKL was refreshed in order to rescue the "physiological state". Figure 12 presents Actin and Hoechst visualization and a specific staining for osteoclasts marker (TRAP) at day 5 of culture. Osteoclastogenesis process is favoured when cultured with osteoblasts, as the process is accelerated[30]. In Mg0.8Ca extract, the process was similar to the scenario presented before (Figure 11) with a less differentiated state. In all PEO-coated material extracts large osteoclasts with many nuclei were obtained, however without marked differences between the PEO-B, PEO-4F and PEO-8F extracts. On the contrary, PEO-9Si extract had the best performance of all, with the whole area covered in large osteoclasts, as disclosed by TRAP staining. In addition, Actin and Hoechst staining showed an intimate presence of osteoblasts around the formed osteoclasts. This fact can be observed in Figure 13, where a merged micrograph at higher magnification is presented; at the

left, an actin ring of a multinucleated formed osteoclast can be seen and at the right, actin cytoskeletons of osteoblasts can be identified.

4. Discussion

4.1. Coating characterization and ion release

…

The differences observed in the electrical response of the PEO process (Figure 1) may be associated with the compositions of the electrolytes[49] and the coatings: the inferior V_{rms} displayed by F-containing electrolytes is related to greater passivation of Mg surface in the presence of fluoride (due to formation of MgF_2). When fluoride-based compounds begin to form [24], coating thickness and impedance increase rapidly resulting in lower voltage.

All the bioactive elements present in the electrolyte were successfully incorporated into the coatings. The addition of Si into the electrolyte has been reported to facilitate more homogeneous coatings and stabilize HA in the coatings [50]. Si typically forms Si-rich top layers related to precipitation of amorphous SiO_2, as shown for PEO coatings of aluminium substrates [51]. The forsterite detected in the present work (Figure 3A) could have been formed by a reaction between MgO and SiO_2 within temperature range of 1100-1400ºC [52]; its presence may have contributed to the enhanced compactness and mechanical properties of the coating (e.g. microhardness). Forsterite has also been related with an improved corrosion resistance of PEO coatings on other Mg alloys [53].

The greater incorporation of F in PEO-8F coating compared with PEO-4F one correlated with the higher concentration of F^- ions in the electrolyte. The location of the species near the barrier layer can be explained by migration of fluoride ions inwards [54] and preferential formation of MgF_2 because of higher concentration of F^- ions in comparison with OH^-.F^- ions cause

passivation of the surface of Mg alloy [55] due to formation of MgF_2; the formation of fluoride-based compounds in the ceramic layer is further assisted by plasma microdischarges. As a result, F-containing coatings presented crystalline phases such as FA which is reported to have bioactivity similar to that of the HA present in bone tissue [56, 57]. The presence of FA (in PEO-4F and PEO-8F) and HA (in PEO-B and PEO-9Si) can be considered as an indicator of potential bioactivity of these coatings.

The liberation of Ca, P, Mg and Si ions measured by ICP (Table 4) was consistent with the area EDS analysis of the coating compositions (Table 1). Mg released from the non-coated substrate (65 to 417 μg $cm^{-2}d^{-1}$) can be attributed solely to the corrosion process. The amount of Mg released into the solution from PEO-coated specimens, on the other hand, includes the ions produced both by the electrochemical corrosion process and by chemical dissolution, i.e. by the lixiviation process. The contribution of the electrochemical corrosion can be measured and corresponds to the amount of the evolved H_2; accordingly, PEO coatings greatly reduce the electrochemical corrosion of Mg, as the authors have shown previously for Mg0.8Ca alloy [10]. Therefore, the much greater release of Mg from PEO-9Si and F-containing coatings compared to the non-coated alloy and to the much thinner PEO-B specimen, can be explained by chemical dissolution of these coatings. The Mg release from the coatings correlates with their thickness and complex phase composition: the thicker coatings (PEO-4F and PEO-8F) containing $MgF_2$and $Mg_2(PO_4)F$ showed the highest liberation. Similarly to Mg release, Ca and P ion liberation was greater from the coatings that contained F, which must be attributed to the coating thickness and the presence of MgF_2, CaF_2 and $Ca_3(PO_4)_5F$ in these coatings.

Regarding the lixiviation mechanism of Ca and P, the low K_{sp} values [58, 59] of HA and FA (6.8×10^{-37} and 5.1×10^{-61}) indicate that these compounds cannot be the principal sources of Ca and P ions in the solution, since the quantities detected in the solution are much higher

(Table 4) than those that can be expected (55.6 ppb Ca and 25.7 ppb P) from K_{sp}. Therefore, this enhanced lixiviation must be attributed to amorphous Ca-P compounds (consistent with the presence of some amorphous material in the coatings as disclosed by XRD, Figure 3) with higher solubility [60]. Mg0.8Ca substrate also contributes from 2.1 to 9.3 μg cm^{-2} d^{-1} of Ca into the medium (Table 4).

Fluoride liberation measurements disclosed a drastic reduction of free F^- in the solution after 5 days. The latter is explained by liberation of other ions from the coating and their reaction with F^- which results in formation of precipitates such as MgF_2, CaF_2, $Mg_2(PO_4)F$ and $Ca_2(PO_4)F$ with low solubility product values. In order to avoid the negative effect of F^- in the organism, its permissible intake is limited by the WHO (World Health Organization) to the range of 1.4-3.4 mg a day. Therefore, the maximum F^- release (118.9 μg cm^{-2}) measured in this work would be within the allowed intake as long as the implant area does not exceed ~10 cm^2. An initial burst of F^- could be expected after the implant makes contact with the physiological medium avoiding a possible initial bacteria colonization.

4.2. Coating biocompatibility

Initial cell biocompatibility was assessed by direct seeding studies and, as expected, cells (endothelial, premyoblastic and preosteoblastic) were not able to proliferate successfully over the non-coated alloy (Figure 4). The increase of the pH of the medium and the formation of H_2bubbles as a result of the corrosion process of Mg reduce the biocompatibility of the material. Nonetheless, premyoblastic line presented higher number of cells growing over the substrate than endothelial line which could be attributed to a greater resistance of the former to the alkalinisation of the medium. The osteoblast cells performance on non-coated substrate corroborates the reports of osteoblastic cells being able to perform in higher pH media compared with other types of cells [61, 62].

In regards to the coating composition, the incorporation of elements such as Ca, P, Si and F into the ceramic PEO layer can be expected to promote different biological responses since i) Ca and P are essential part of bone mineralization; ii) F can provide antibacterial properties and even favour osteogenesis process [63], although it can affect endothelial cells negatively in concentration-dependent manner [47]; iii) Si promotes vascularization and bone regeneration. Along with the action of the Mg itself, these elements can favour bone regeneration processes or other biological processes. For instance, besides its implication in bone tissue, Ca is important in signalling. It is known that positively charged Ca^{2+} and negatively charged phosphate ions are two primary signalling elements of cells. Ca^{2+} binds to thousands of proteins to produce changes in localization, association, and function [64]. Moreover, endothelial Ca decreases with age and its signalling in endothelial cells is essential to vasomotor control.

In relation to PEO coatings bioactivity, the F-containing coatings showed a reduced monolayer formation of the preosteoblastic cells, unlike PEO-B and PEO-9Si, which may be due to the presence of fluoride as well as the greater roughness of both PEO-4F and PEO-8F coatings with R_a values around 4 µm (Table 2). The latter fact contrasts with the good performance of the preosteoblastic cells in terms of monolayer formation on the smoother surfaces of PEO-B and PEO-9Si with R_a values less than 1 µm (Table 2), suggesting that a less uneven topography and the incorporation into the ceramic coating of Ca, P or Si is preferential for the ability to proliferate over the material. Both topographical features and chemical composition can highly influence in the final behaviour of these cells. As for endothelial cells, there was a differential behaviour between F-containing coatings as PEO-8F coating did not seem to be disturbing them to the same extent as PEO-4F, which could possibly be related to the steeper decrease of free F^- in the media with time in case of PEO-8F (Table 4) allowing the cells to form a monolayer. Premyoblastic cells were the most robust cell line evaluated and all the cell lines presented the best performance onPEO-9Si even with better results than for Ti CP positive control.

PEO-9Si also stood out with the best performance in extracts biocompatibility studies with significant statistical results for C2C12-GFP in both 1:2 and 1:10 dilution conditions. Considering that the content of released Mg in the latter is as low as ~0.8 ppm suggests that (i) cells are sensitive even to minor amounts of Si and (ii) are relatively indifferent to a large variation of Mg concentration in the media, provided that a favourable pH is maintained, since no correlation is observed between the Mg content and the metabolic activity. Si is considered a favouring element in angiogenesis processes [65] explaining the good behaviour of PEO-9Si coating and suggesting the possible positive implications after implantation of the material in the vascularization of tissues. Moreover, the implication of Si in bone metabolism and promotion of bone regeneration has been widely described [23, 24] and the present findings are in agreement with other works where Si has been incorporated into a biomaterial and the same cell line was used [24].

Interestingly, in 1:2 extracts (Figure 7) similarly poor results were obtained for Mg0.8Ca and PEO-8F showing very low biocompatibility with the endothelial cell line (C166-GFP). Whereas in case of Mg0.8Ca this is related to the high pH of the extract, for PEO-8F this could be explained by the fluoride cytotoxicity observed for C166-GFP (Supplementary Figure 2), as PEO-8F shows the highest release of F^- at short times. The F^- concentration in the PEO-8F 1:2 diluted extract can be estimated as ~44 ppm or ~2.3 mM, which is above the F- tolerance limit determined initially.

In regards to the tendencies observed in the differentiation studies, PEO-9Si extracts favoured the differentiation markers, e.g. calcium deposits were rounded and bigger-sized (Figure 10). Si can positively influence osteoblast differentiation, increasing or accelerating this process. Moreover, in the co-culture studies PEO-9Si favoured the osteoclastogenesis process among all the evaluated conditions. It is known that an acidic environment is needed for fusion and

expansion of mature osteoclasts [61, 66], which may explain why PEO-9Si, which produced less changes in the pH, favoured the differentiation processes.

5. Conclusions

Four ceramic-like coatings were fabricated on Mg0.8Ca alloy by AC PEO from Ca- and P-containing electrolytes with added Si or F. Biocompatible compounds such as hydroxyapatite and fluorapatite were formed in all the coatings. The incorporation of species such as fluoride was found to be critical for endothelial cells. Surface characteristics of PEO coatings (roughness, porosity) were determinant for their *in vitro* response and were dependent of the chemical composition of the electrolyte. The coatings with high roughness ($R_a \geq 3.6$) and a high F content (~9-11 at.%) limited the formation of a structured monolayer of preosteoblastic and endothelial cells. An improved bioactivity of PEO-9Si with respect to all the evaluated cell lines was associated with its chemical composition, favourable surface characteristics and corrosion protection, associated with its elevated compactness. The 1:2 extracts compromised the viability of C166-GFP and C2C12-GFP cell lines. The diluted extracts (1:10) derived from the PEO coatings tended to improve the metabolic activity in comparison with the positive control; an enhanced metabolic activity of premyoblastic cells in PEO-9Si extract being linked with the minor presence of Si in the extract. All 1:4 diluted extracts allowed osteoblastic differentiation. Improved collagen secretion and mineralization were found in Si-containing extract compared with Si-free and F-containing extracts. Osteoblast and osteoclasts co-culture studies revealed an exceptional behaviour of both cell types in PEO-9Si extract. To sum up, the incorporation of Si into the ceramic coating seemed to be a critical feature improving their bioactive properties, showing the potential of this new PEO coating for biodegradable implant applications.

Acknowledgments

This work was funded by Regional Government of Madrid and EU Structural Funds (S2013/MIT-2862-CM, P2018/NMT-4411). A. Santos-Coquillat is grateful to Youth Employment Initiative (YEI) of Regional Government of Madrid and EU Social Funds for financial support (PEJD-2016/IND-3095). M. Mohedano gratefully acknowledges the support of MINECO (MAT20I5-733 55-JIN).

References

[1] P. Tian, X. Liu, Regenerative Biomaterials, 2 (2015) 135-151.

[2] A. Atrens, G.-L. Song, F. Cao, Z. Shi, P.K. Bowen, Journal of Magnesium and Alloys, 1 (2013) 177-200.

[3] M. Nabiyouni, T. Brückner, H. Zhou, U. Gbureck, S.B. Bhaduri, Acta Biomaterialia, 66 (2018) 23-43.

[4] F. Witte, Acta Biomaterialia, 6 (2010) 1680-1692.

[5] T. Kraus, S. Fischerauer, S. Treichler, E. Martinelli, J. Eichler, A. Myrissa, S. Zötsch, P.J. Uggowitzer, J.F. Löffler, A.M. Weinberg, Acta Biomaterialia, 66 (2018) 109-117.

[6] S. You, Y. Huang, K.U. Kainer, N. Hort, Journal of Magnesium and Alloys, 5 (2017) 239-253.

[7] A. Atrens, S. Johnston, Z. Shi, M.S. Dargusch, Scripta Materialia, 154 (2018) 92-100.

[8] R. Radha, D. Sreekanth, Journal of Magnesium and Alloys, 5 (2017) 286-312.

[9] X.N. Gu, W. Zheng, Y. Cheng, Y.F. Zheng, Acta Biomaterialia, 5 (2009) 2790-2799.

[10] M. Mohedano, B.J.C. Luthringer, B. Mingo, F. Feyerabend, R. Arrabal, P.J. Sanchez-Egido, C. Blawert, R. Willumeit-Römer, M.L. Zheludkevich, E. Matykina, Surface and Coatings Technology, 315 (2017) 454-467.

[11] G.J. Wan, M.F. Maitz, H. Sun, P.P. Li, N. Huang, Surface and Coatings Technology, 201 (2007) 8267-8272.

[12] P. Amaravathy, S. Sowndarya, S. Sathyanarayanan, N. Rajendran, Surface and Coatings Technology, 244 (2014) 131-141.

[13] D. Chen, E.H. Jordan, M. Gell, M. Wei, Acta Biomaterialia, 4 (2008) 553-559.

[14] H.R. Bakhsheshi-Rad, M.H. Idris, M.R. Abdul-Kadir, Surface and Coatings Technology, 222 (2013) 79-89.

[15] A. Mahapatro, S.A. Arshanapalli, Journal of Bio- and Tribo-Corrosion, 3 (2017) 37.

[16] H. Hornberger, S. Virtanen, A.R. Boccaccini, Acta Biomaterialia, 8 (2012) 2442-2455.

[17] A.S. Gnedenkov, S.L. Sinebryukhov, D.V. Mashtalyar, S.V. Gnedenkov, Corrosion Science, 102 (2016) 269-278.

[18] M. Sun, A. Yerokhin, M.Y. Bychkova, D.V. Shtansky, E.A. Levashov, A. Matthews, Corrosion Science, 111 (2016) 753-769.

[19] R. Zhou, D. Wei, J. Cao, W. Feng, S. Cheng, Q. Du, B. Li, Y. Wang, D. Jia, Y. Zhou, ACS Applied Materials & Interfaces, 7 (2015) 8932-8941.

[20] T.S.N. Sankara Narayanan, I.S. Park, M.H. Lee, Progress in Materials Science, 60 (2014) 1-71.

[21] R.-C. Zeng, L.-y. Cui, K. Jiang, R. Liu, B.-D. Zhao, Y.-F. Zheng, ACS Applied Materials & Interfaces, 8 (2016) 10014-10028.

[22] X.N. Gu, N. Li, W.R. Zhou, Y.F. Zheng, X. Zhao, Q.Z. Cai, L. Ruan, Acta Biomaterialia, 7 (2011) 1880-1889.

[23] R. Jugdaohsingh, The journal of nutrition, health & aging, 11 (2007) 99-110.

[24] E.J. Kim, S.Y. Bu, M.K. Sung, M.K. Choi, Biological trace element research, 152 (2013) 105-112.

[25] T. Zhang, X. Wu, H. Huang, Y. Zhang, M. Li, G. Lan, H. Xia, Q. Yin, Materials Letters, 137 (2014) 362-365.

[26] Z. Zhang, J. Sun, H. Hu, Q. Wang, X. Liu, Journal of Biomedical Materials Research Part B: Applied Biomaterials, 97B (2011) 224-234.

[27] L. Wu, F. Feyerabend, A.F. Schilling, R. Willumeit-Romer, B.J.C. Luthringer, Acta Biomater, 27 (2015) 294-304.

[28] C.M. Botelho, R.A. Brooks, G. Spence, I. McFarlane, M.A. Lopes, S.M. Best, J.D. Santos, N. Rushton, W. Bonfield, Journal of biomedical materials research. Part A, 78 (2006) 709-720.

[29] Y.-K. Kim, Y.-S. Jang, Y.-H. Lee, H.-K. Yi, T.-S. Bae, M.-H. Lee, Scientific Reports, 7 (2017) 712.

[30] G.L. Jones, A. Motta, M.J. Marshall, A.J. El Haj, S.H. Cartmell, Biomaterials, 30 (2009) 5376-5384.

[31] F. Witte, V. Kaese, H. Haferkamp, E. Switzer, A. Meyer-Lindenberg, C.J. Wirth, H. Windhagen, Biomaterials, 26 (2005) 3557-3563.

[32] H. Waizy, J. Diekmann, A. Weizbauer, J. Reifenrath, I. Bartsch, V. Neubert, R. Schavan, H. Windhagen, Journal of Biomaterials Applications, 28 (2014) 667-675.

[33] D. Mushahary, C. Wen, J.M. Kumar, J. Lin, N. Harishankar, P. Hodgson, G. Pande, Y. Li, Colloids and Surfaces B: Biointerfaces, (2014).

[34] X. Lin, L. Tan, Q. Wang, G. Zhang, B. Zhang, K. Yang, Materials Science and Engineering: C, 33 (2013) 3881-3888.

[35] S.F. Fischerauer, T. Kraus, X. Wu, S. Tangl, E. Sorantin, A.C. Hänzi, J.F. Löffler, P.J. Uggowitzer, A.M. Weinberg, Acta Biomaterialia, 9 (2013) 5411-5420.

[36] Y. Chen, J. Yan, X. Wang, S. Yu, Z. Wang, X. Zhang, S. Zhang, Y. Zheng, C. Zhao, Q. Zheng, BioMetals, (2014).

[37] J.X. Yang, F.Z. Cui, I.S. Lee, Y. Zhang, Q.S. Yin, H. Xia, S.X. Yang, Journal of Biomaterials Applications, 27 (2012) 153-164.

[38] X. Xiao, H. Yu, Q. Zhu, G. Li, Y. Qu, R. Gu, Journal of Bionic Engineering, 10 (2013) 156-161.

[39] D. Mushahary, R. Sravanthi, Y. Li, M.J. Kumar, N. Harishankar, P.D. Hodgson, C. Wen, G. Pande, International Journal of Nanomedicine, 8 (2013) 2887-2902.

[40] T. Imwinkelried, S. Beck, T. Iizuka, B. Schaller, Acta Biomaterialia, 9 (2013) 8643-8649.

[41] A. Santos-Coquillat, R. Gonzalez Tenorio, M. Mohedano, E. Martinez-Campos, R. Arrabal, E. Matykina, Applied Surface Science.

[42] M.R. Katunar, A. Gomez Sanchez, A. Santos Coquillat, A. Civantos, E. Martinez Campos, J. Ballarre, T. Vico, M. Baca, V. Ramos, S. Cere, Materials Science and Engineering: C, 75 (2017) 957-968.

[43] E. Martínez-Campos, T. Elzein, A. Bejjani, M.J. García-Granda, A. Santos-Coquillat, V. Ramos, A. Muñoz-Bonilla, J. Rodríguez-Hernández, ACS Applied Materials & Interfaces, 8 (2016) 6344-6353.

[44] H. Li, W. He, S. Pang, P.K. Liaw, T. Zhang, Materials Science and Engineering: C, 68 (2016) 632-641.

[45] J. Fei, X. Wen, X. Lin, Saijilafu, W. Wang, O. Ren, X. Chen, L. Tan, K. Yang, H. Yang, L. Yang, Materials Science and Engineering: C, 78 (2017) 1155-1163.

[46] C. Pérez-Jorge, A. Conde, M.A. Arenas, R. Pérez-Tanoira, E. Matykina, J.J. de Damborenea, E. Gómez-Barrena, J. Esteban, Journal of Biomedical Materials Research Part A, 100A (2012) 1696-1705.

[47] M. Szczepanski, M. Kamianowska, G. Kamianowski, Oral diseases, 18 (2012) 280-284.

[48] P. Collin-Osdoby, P. Osdoby, Methods in molecular biology (Clifton, N.J.), 816 (2012) 187-202.

[49] S. Ikonopisov, Electrochimica Acta, 22 (1977) 1077-1082.

[50] A.F. Khan, M. Saleem, A. Afzal, A. Ali, A. Khan, A.R. Khan, Materials Science and Engineering: C, 35 (2014) 245-252.

[51] F. Monfort, A. Berkani, E. Matykina, P. Skeldon, G.E. Thompson, H. Habazaki, K. Shimizu, Corrosion Science, 49 (2007) 672-693.

[52] G.W. Brindley, R. Hayami, The Philosophical Magazine: A Journal of Theoretical Experimental and Applied Physics, 12 (1965) 505-514.

[53] J. Liu, Y. Lu, X. Jing, Y. Yuan, M. Zhang, Materials and Corrosion, 60 (2009) 865-870.

[54] H. Habazaki, K. Fushimi, K. Shimizu, P. Skeldon, G.E. Thompson, Electrochemistry Communications, 9 (2007) 1222-1227.

[55] M. Carboneras, M.C. García-Alonso, M.L. Escudero, Corrosion Science, 53 (2011) 1433-1439.

[56] S.V. Dorozhkin, Biomaterials, 31 (2010) 1465-1485.

[57] C.J. Tredwin, A.M. Young, E.A. Abou Neel, G. Georgiou, J.C. Knowles, Journal of materials science. Materials in medicine, 25 (2014) 47-53.

[58] L.C. Bell, H. Mika, B.J. Kruger, Archives of Oral Biology, 23 (1978) 329-336.

[59] H.G. McCann, Archives of Oral Biology, 13 (1968) 987-1001.

[60] M. Mohedano, R. Guzman, R. Arrabal, J.-L. Lopez Lacomba, E. Matykina, Journal of Biomedical Materials Research, Part B: Applied Biomaterials, 101 (2013) 1524-1537.

[61] T.R. Arnett, The Journal of Nutrition, 138 (2008) 415S-418S.

[62] Y. Shen, W. Liu, C. Wen, H. Pan, T. Wang, B.W. Darvell, W.W. Lu, W. Huang, Journal of Materials Chemistry, 22 (2012) 8662-8670.

[63] X. Ge, Y. Leng, C. Bao, L. Xu Sherry, R. Wang, F. Ren, Journal of Biomedical Materials Research Part A, 95A (2010) 588-599.

[64] D.E. Clapham, Cell, 131 (2007) 1047-1058.

[65] H. Li, J. Chang, Acta biomaterialia, 9 (2013) 6981-6991.

[66] T. Nordstrom, O.D. Rotstein, R. Romanek, S. Asotra, J.N. Heersche, M.F. Manolson, G.F. Brisseau, S. Grinstein, The Journal of biological chemistry, 270 (1995) 2203-2212.

Figure captions

Figure 1. Voltage-time dependencies for the formation of PEO coatings on Mg0.8Ca alloy.

Figure 2. Secondary electron plan view micrographs and backscattered electron cross-sectional micrographs of the PEO coatings (PEO-B, PEO-4F, PEO-8F and PEO-9Si). Numbers indicate where the local EDS analysis (Table 2) was performed.

Figure 3. A. X-Ray diffraction patterns for the PEO coatings. **B.**X-Ray diffraction patterns after 5 days of exposure in DMEM.

Figure 4. Cells growing over the PEO-coated materials and control materials, Mg0.8Ca and Ti CP, for 5 days. **A.** Fluorescence micrographs of C166-GFP and C2C12-GFP cell lines. **B.**Actin (red) and Hoechst (blue) of MC3T3 preosteoblastic cell line.

Figure 5. Secondary electron micrographs of C2C12-GFP preomyoblastic cell line spreading in the PEO-coated Mg0.8Ca alloy after 5 days of culture.

Figure 6. Optical micrographs, variation of surface topography and 3D-rendering of the surface of non-coated and coated Mg0.8Ca after 5 days of exposure in DMEM.

Figure 7. Extracts cytocompatibility. **A.** Micrographs of C166-GFP and C2C12-GFP cells after 5 days in contact with 1:2 extracts. **B**. AlamarBlue results at day 5 of both cell lines incubated with extracts 1:2. Each extract condition is compared with control bare material for each cell line.

Figure 8. Extracts cytocompatibility. **A.** Optical micrographs of C166-GFP and C2C12-GFP cells after 5 days in contact with 1:10 extracts. **B.** AlamarBlue results at day 5 of both cell lines

incubated with extracts 1:10. Each extract condition is compared with control bare material for each cell line.

Figure 9. **A.** Sirius red staining after 14 days of culture **B.** Colorimetric quantification **C.** Detailed morphology of PEO-9Si staining.

Figure 10. Mineralization study. Alizarin red staining of MC3T3 cells after 7 days of 1:4 extract incubation and 14 days of culture.

Figure 11. TRAP staining. Osteoclast differentiation after 5 days of incubation in 1:4 extracts (the medium and RANKL refreshed after day 3).

Figure 12. Co-cultures of osteoblasts and osteoclasts (MC3T3 and RAW 364.7 cells) with extracts 1:4. Left row - actin cytoskeleton staining, center row - nuclei staining by Hoechst, right row - TRAP staining for resorption marker expression.

Figure 13. Merged of Actin and Hoechst staining of co-cultured RAW 364.7 and MC3T3 cells with 1:4 PEO-9Si extract.

Table 1. Chemical composition, pH and conductivity of PEO electrolytes.

Table 2. Local EDS analysis of the coatings (at. %) at the locations in the micrographs presented in Figure 2.

Table 3. Surface characteristics of the studied coatings.

Table 4. Ion liberation from coatings and bare alloy after 5 days of immersion in 0.9 wt.% NaCl determined by ICP-OES.

Table 5. Ion liberation from coatings after 1 and 5 days immersion in 0.9 wt.% NaCl determined by Ion Selective Electrode (ISE).

Supplementary Figure 1. Mg0.8Ca alloy (1×1 cm^2) after 5 days of immersion in 0.9% NaCl.

Supplementary Figure 2. Endothelial C166-GFP and premyoblastic C2C12-GFP cells growing over the bare alloy (Mg0.8Ca), control Ti CP and the ceramic coatings (PEO-B, PEO-4F, PEO-8F and PEO-9Si) after 24 h of seeding.

Supplementary Figure 3. NaF cytotoxicity study with C166-GFP, C2C12-GFP and MC3T3 cell lines. Each condition was compared with the the non-treated control for each cell line.

Supplementary Figure 4. A. Metabolic activity evaluation of MC3T3 cells after 7 days growing in contact with 1:4 extracts. **B.** Sirius Red quantification at day 7 of culture. Each extract condition is compared with control bare material (Mg0.8Ca) for each cell line.

Figure captions

Figure 1. Voltage-time dependencies for the formation of PEO coatings on Mg0.8Ca alloy.

Figure 2. Secondary electron plan view micrographs and backscattered electron cross-sectional micrographs of the PEO coatings (PEO-B, PEO-4F, PEO-8F and PEO-9Si). Numbers indicate where the local EDS analysis (Table 2) was performed.

Figure 3. A. X-Ray diffraction patterns for the PEO coatings. **B.**X-Ray diffraction patterns after 5 days of exposure in DMEM.

Figure 4. Cells growing over the PEO-coated materials and control materials, Mg0.8Ca and Ti CP, for 5 days. **A.** Fluorescence micrographs of C166-GFP and C2C12-GFP cell lines. **B.**Actin (red) and Hoechst (blue) of MC3T3 preosteoblastic cell line.

Figure 5. Secondary electron micrographs of C2C12-GFP preomyoblastic cell line spreading in the PEO-coated Mg0.8Ca alloy after 5 days of culture.

Figure 6. Optical micrographs, variation of surface topography and 3D-rendering of the surface of non-coated and coated Mg0.8Ca after 5 days of exposure in DMEM.

Figure 7. Extracts cytocompatibility. **A.** Micrographs of C166-GFP and C2C12-GFP cells after 5 days in contact with 1:2 extracts. **B**. AlamarBlue results at day 5 of both cell lines incubated with extracts 1:2. Each extract condition is compared with control bare material for each cell line.

Figure 8. Extracts cytocompatibility. **A.** Optical micrographs of C166-GFP and C2C12-GFP cells after 5 days in contact with 1:10 extracts. **B.** AlamarBlue results at day 5 of both cell lines incubated with extracts 1:10. Each extract condition is compared with control bare material for each cell line.

Figure 9. **A.** Sirius red staining after 14 days of culture **B.** Colorimetric quantification **C.** Detailed morphology of PEO-9Si staining.

Figure 10. Mineralization study. Alizarin red staining of MC3T3 cells after 7 days of 1:4 extract incubation and 14 days of culture.

Figure 11. TRAP staining. Osteoclast differentiation after 5 days of incubation in 1:4 extracts (the medium and RANKL refreshed after day 3).

Figure 12. Co-cultures of osteoblasts and osteoclasts (MC3T3 and RAW 364.7 cells) with extracts 1:4. Left row - actin cytoskeleton staining, center row - nuclei staining by Hoechst, right row - TRAP staining for resorption marker expression.

Figure 13. Merged of Actin and Hoechst staining of co-cultured RAW 364.7 and MC3T3 cells with 1:4 PEO-9Si extract.

Table 1. Chemical composition, pH and conductivity of PEO electrolytes.

Table 2. Local EDS analysis of the coatings (at. %) at the locations in the micrographs presented in Figure 2.

Table 3. Surface characteristics of the studied coatings.

Table 4. Ion liberation from coatings and bare alloy after 5 days of immersion in 0.9 wt.% NaCl determined by ICP-OES.

Table 5. Ion liberation from coatings after 1 and 5 days immersion in 0.9 wt.% NaCl determined by Ion Selective Electrode (ISE).

Supplementary Figure 1. Mg0.8Ca alloy (1×1 cm^2) after 5 days of immersion in 0.9% NaCl.

Supplementary Figure 2. Endothelial C166-GFP and premyoblastic C2C12-GFP cells growing over the bare alloy (Mg0.8Ca), control Ti CP and the ceramic coatings (PEO-B, PEO-4F, PEO-8F and PEO-9Si) after 24 h of seeding.

Supplementary Figure 3. NaF cytotoxicity study with C166-GFP, C2C12-GFP and MC3T3 cell lines. Each condition was compared with the the non-treated control for each cell line.

Supplementary Figure 4. A. Metabolic activity evaluation of MC3T3 cells after 7 days growing in contact with 1:4 extracts. **B.** Sirius Red quantification at day 7 of culture. Each extract condition is compared with control bare material (Mg0.8Ca) for each cell line.

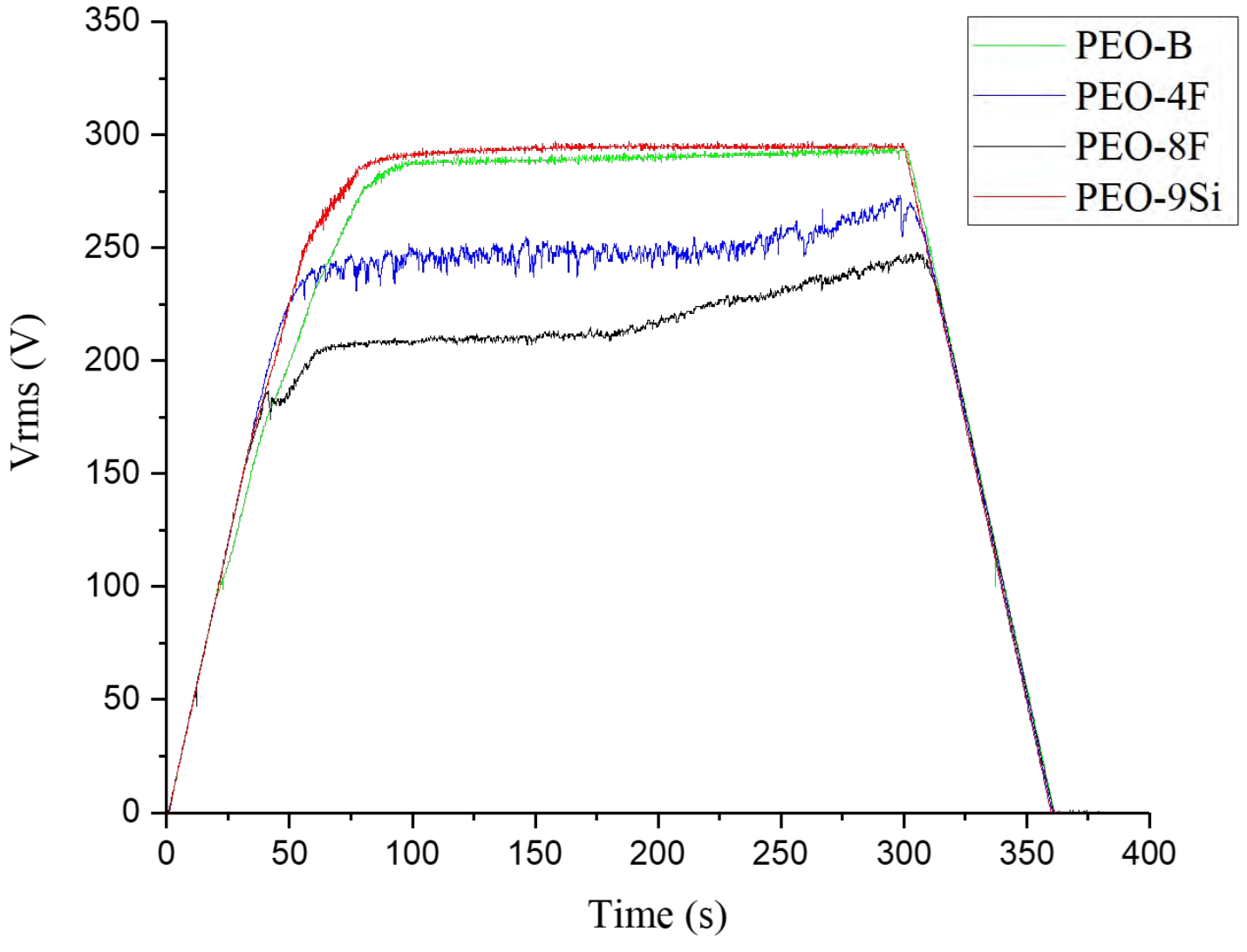
PEO-B
PEO-4F
PEO-8F
PEO-9Si
Vrms (V)
Time (s)
0
50
100
150
200
250
300
350
400

PEO-B
1
100 µm
2
10 µm
PEO-4F
3
100 µm
4
5
30 µm
PEO-8F
6
100 µm
7
8
50 µm
PEO-9Si
9
100 µm
10
11
10 µm

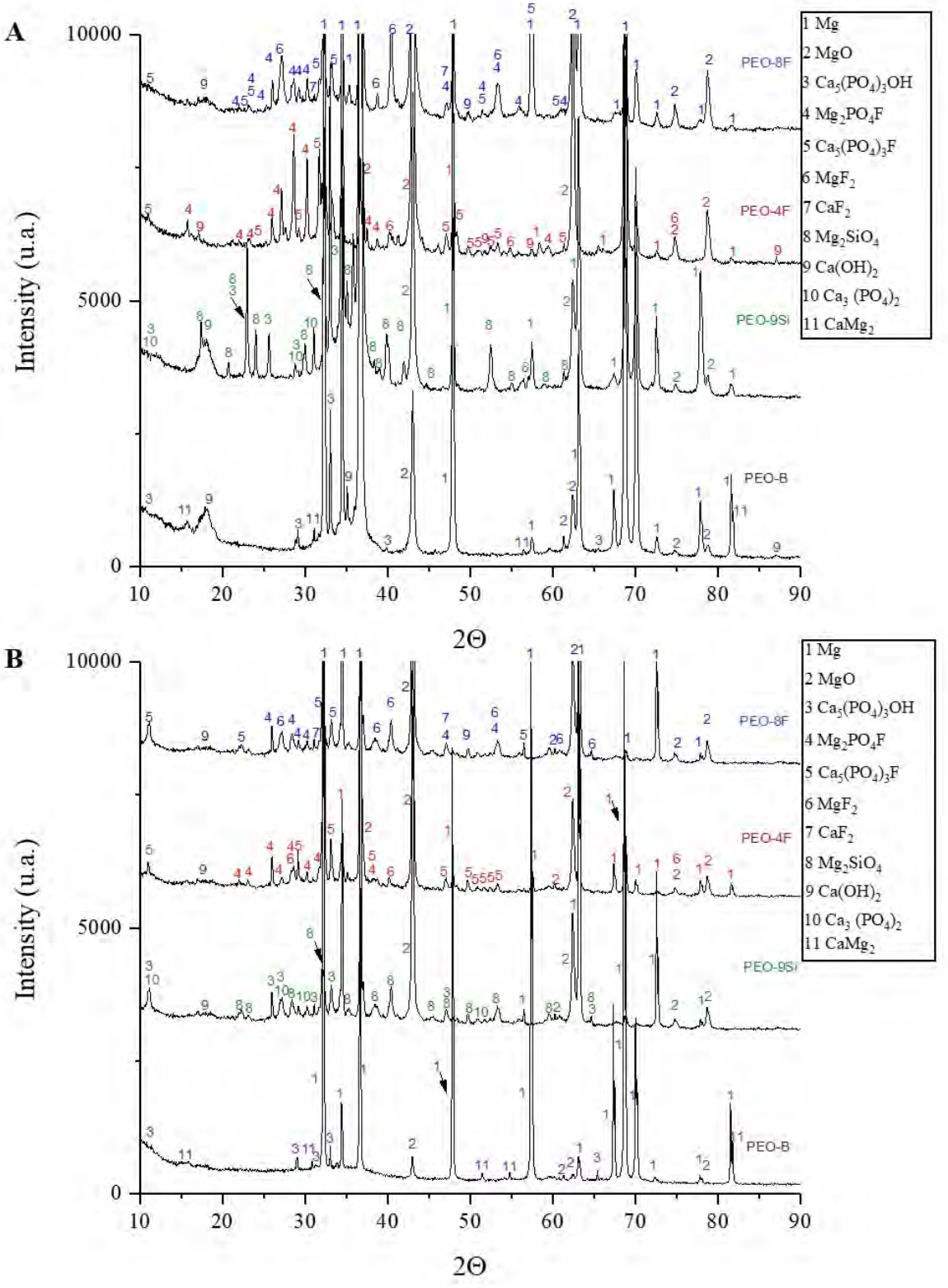
A
B
Intensity (u.a.)
2Θ
PEO-8F
PEO-4F
PEO-9Si
PEO-B
1 Mg
2 MgO
3 $Ca_5(PO_4)_3OH$
4 Mg_2PO_4F
5 $Ca_5(PO_4)_3F$
6 MgF_2
7 CaF_2
8 Mg_2SiO_4
9 $Ca(OH)_2$
10 $Ca_3(PO_4)_2$
11 $CaMg_2$

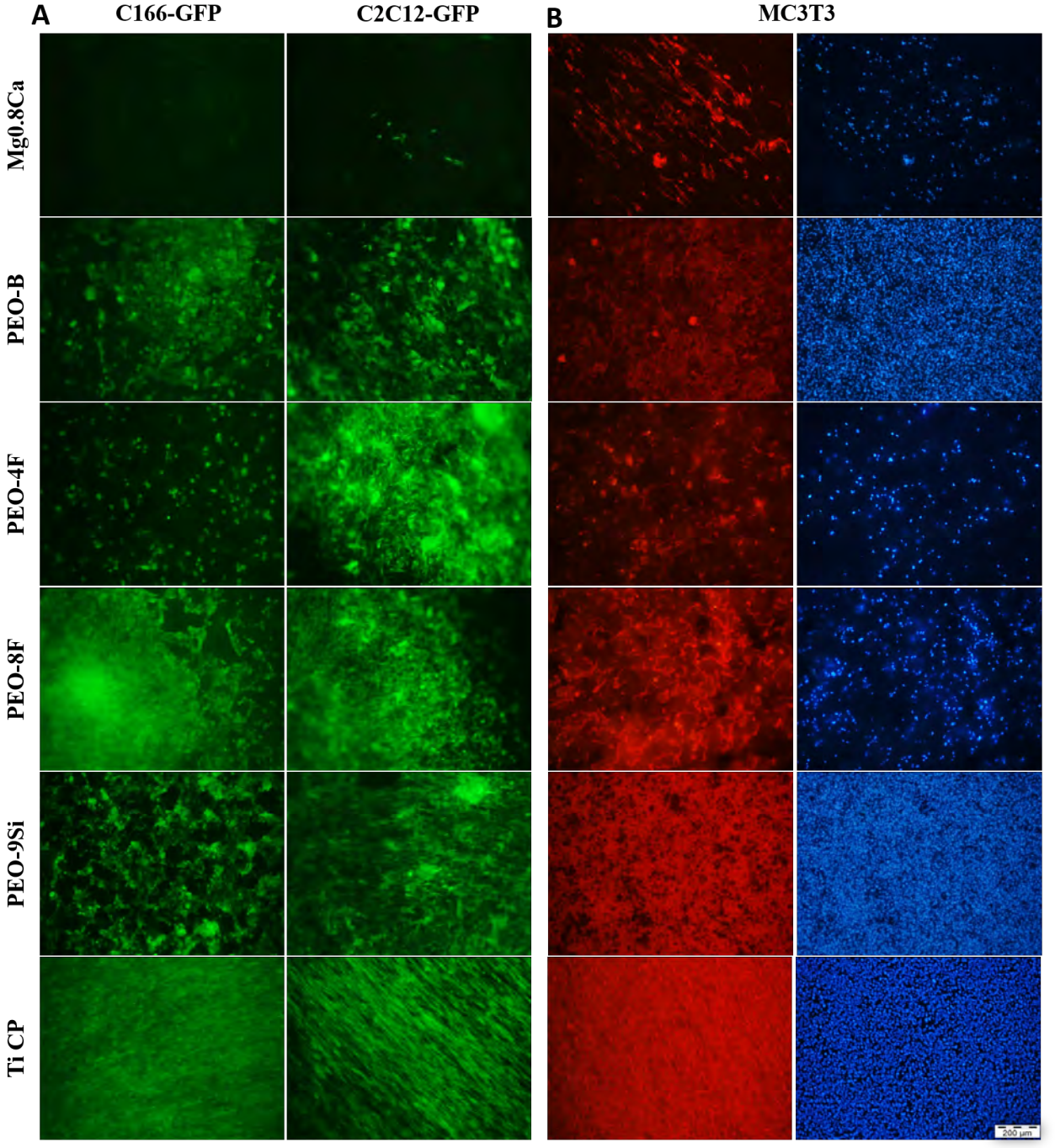
A
C166-GFP
C2C12-GFP
B
MC3T3
Mg0.8Ca
PEO-B
PEO-4F
PEO-8F
PEO-9Si
Ti CP
200 µm

PEO-B
80 µm
100 µm
PEO-4F
80 µm
100 µm
PEO-8F
80 µm
100 µm
PEO-9Si
80 µm
100 µm

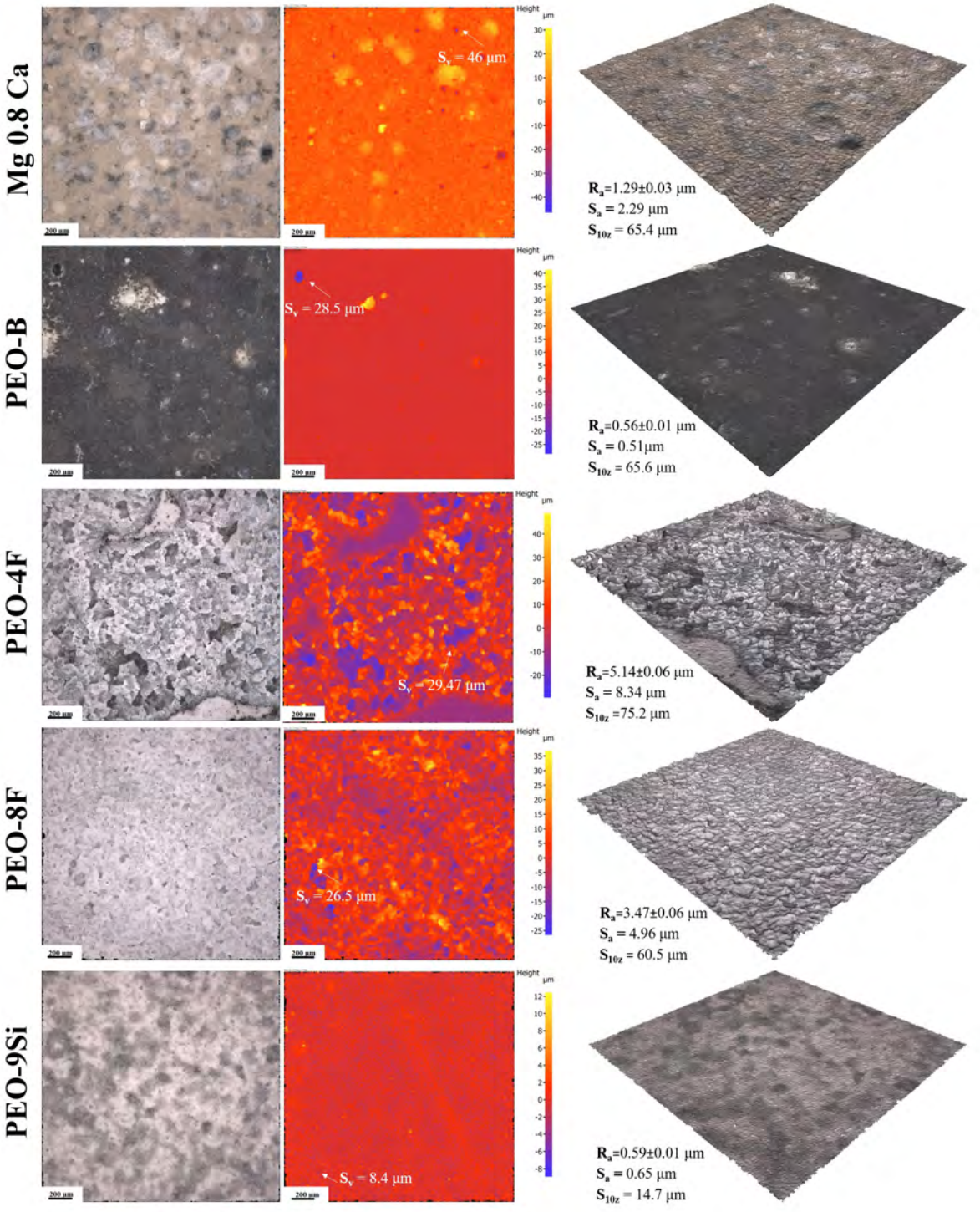
Mg 0.8 Ca
PEO-B
PEO-4F
PEO-8F
PEO-9Si
200 µm
Height µm
S_v = 46 µm
S_v = 28.5 µm
S_v = 29.47 µm
S_v = 26.5 µm
S_v = 8.4 µm
R_a=1.29±0.03 µm
S_a = 2.29 µm
S_{10z} = 65.4 µm
R_a=0.56±0.01 µm
S_a = 0.51µm
S_{10z} = 65.6 µm
R_a=5.14±0.06 µm
S_a = 8.34 µm
S_{10z} =75.2 µm
R_a=3.47±0.06 µm
S_a = 4.96 µm
S_{10z} = 60.5 µm
R_a=0.59±0.01 µm
S_a = 0.65 µm
S_{10z} = 14.7 µm

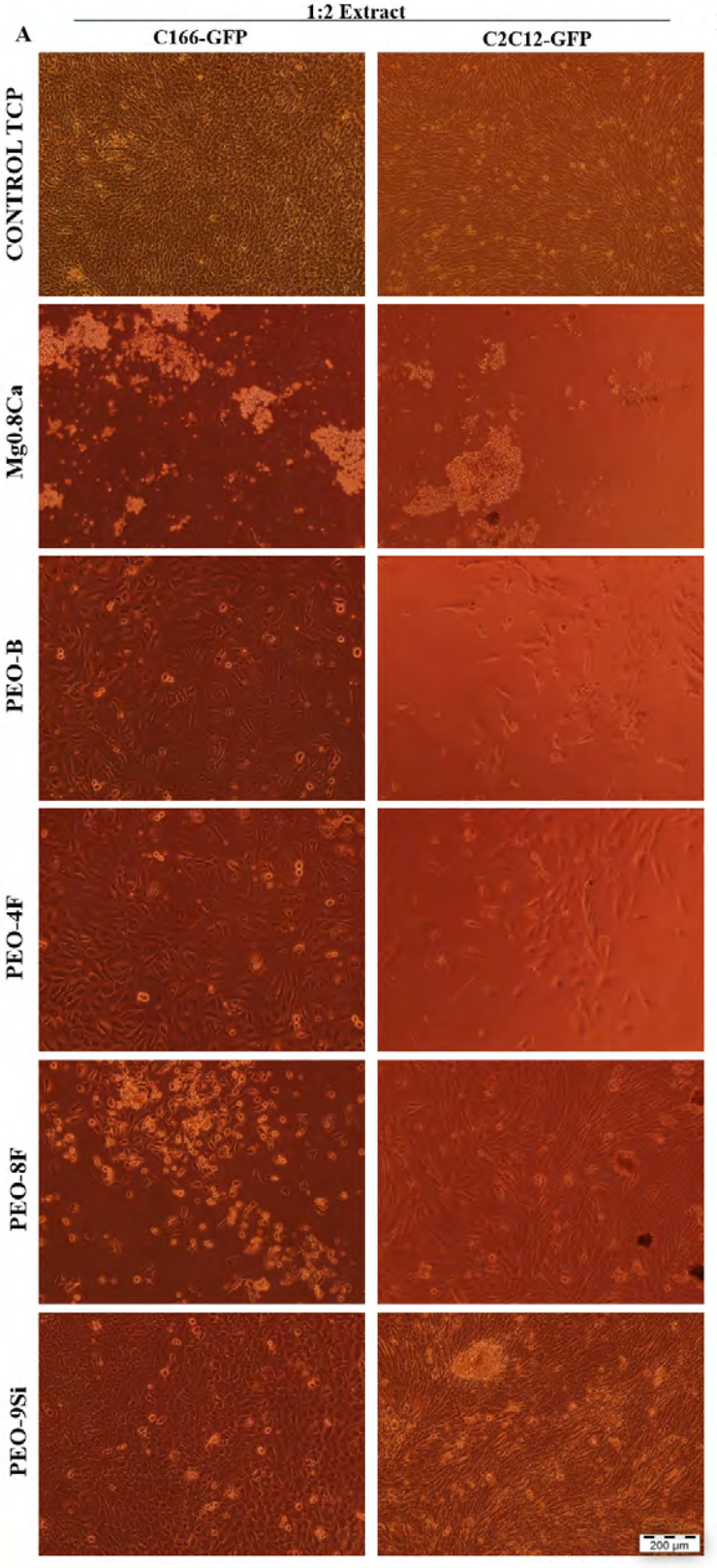
A
1:2 Extract
C166-GFP
C2C12-GFP
CONTROL TCP
Mg0.8Ca
PEO-B
PEO-4F
PEO-8F
PEO-9Si
200 µm

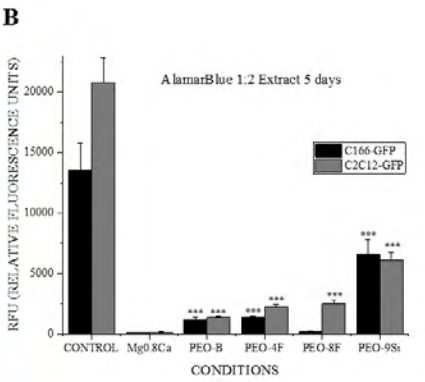
B
AlamarBlue 1:2 Extract 5 days
RFU (RELATIVE FLUORESCENCE UNITS)
20000
15000
10000
5000
0
C166-GFP
C2C12-GFP
***
CONTROL
Mg0.8Ca
PEO-B
PEO-4F
PEO-8F
PEO-9Si
CONDITIONS

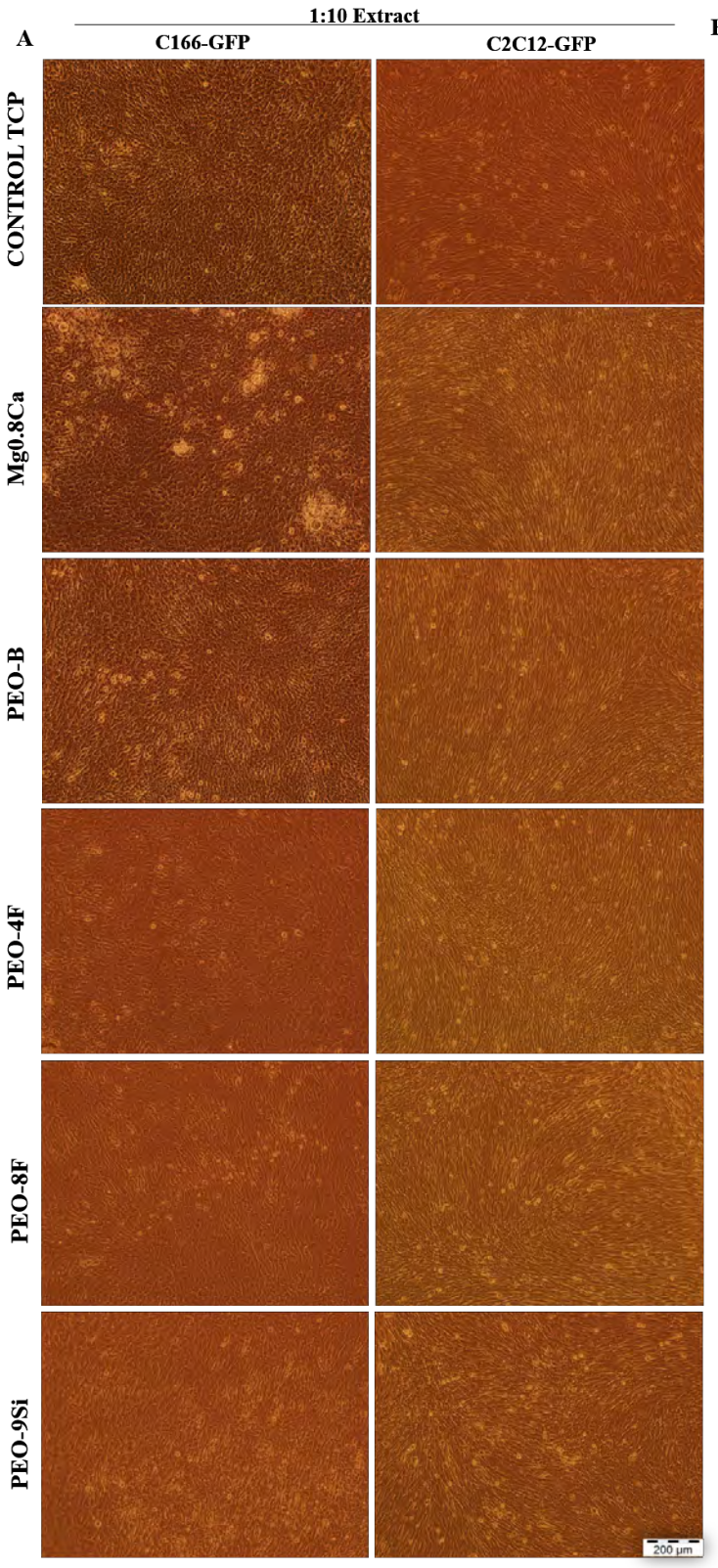
A
1:10 Extract
C166-GFP
C2C12-GFP
CONTROL TCP
Mg0.8Ca
PEO-B
PEO-4F
PEO-8F
PEO-9Si
200 µm

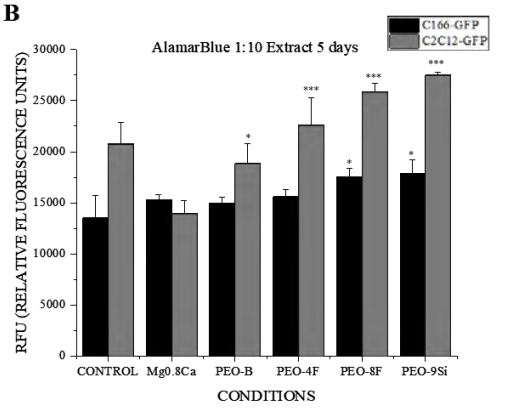
B
AlamarBlue 1:10 Extract 5 days
C166-GFP
C2C12-GFP
RFU (RELATIVE FLUORESCENCE UNITS)
30000
25000
20000
15000
10000
5000
0
CONTROL
Mg0.8Ca
PEO-B
PEO-4F
PEO-8F
PEO-9Si
CONDITIONS

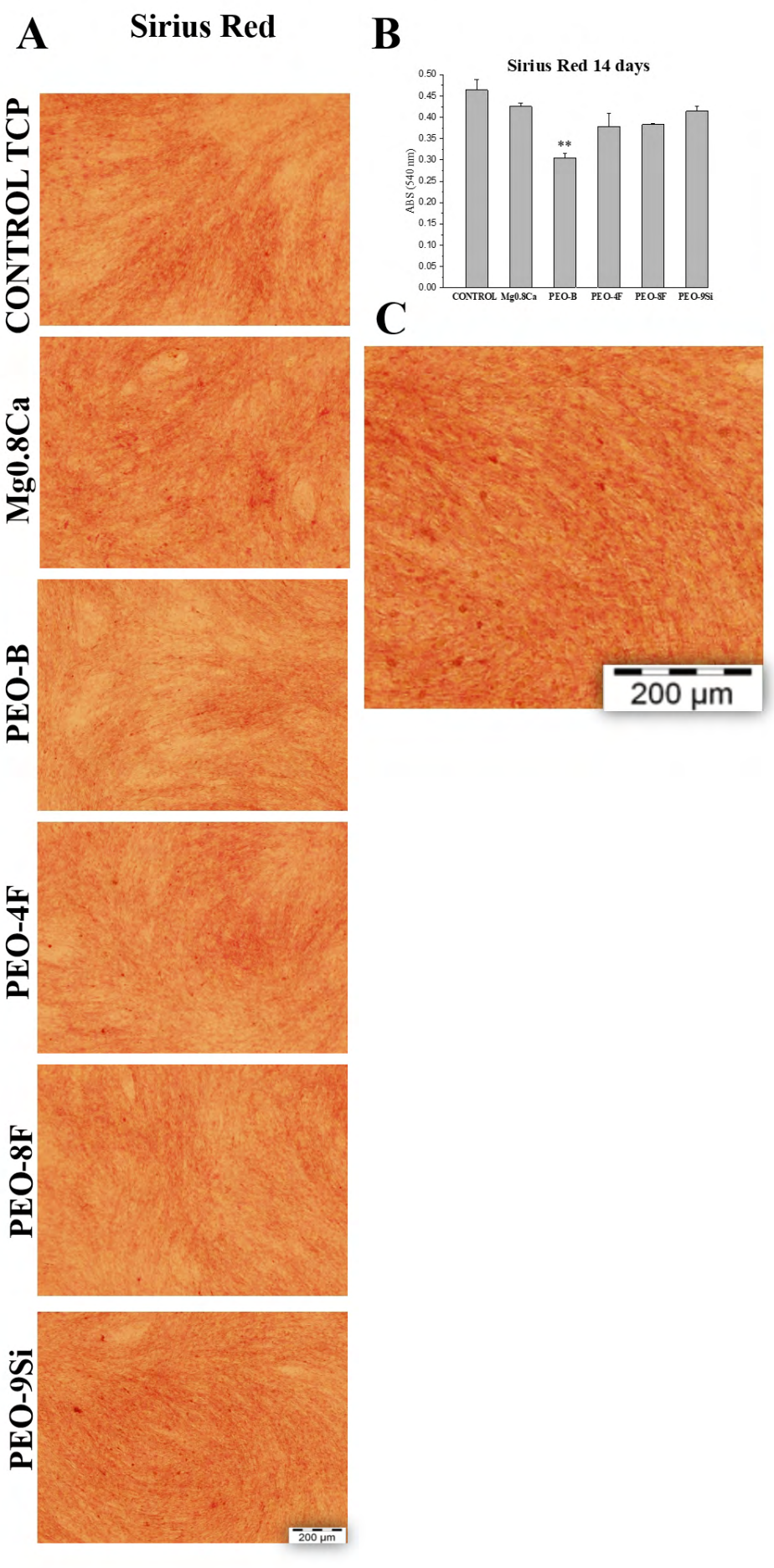
A
Sirius Red
CONTROL TCP
Mg0.8Ca
PEO-B
PEO-4F
PEO-8F
PEO-9Si
200 µm
B
Sirius Red 14 days
ABS (540 nm)
0.50
0.45
0.40
0.35
0.30
0.25
0.20
0.15
0.10
0.05
0.00
**
CONTROL
Mg0.8Ca
PEO-B
PEO-4F
PEO-8F
PEO-9Si
C
200 µm

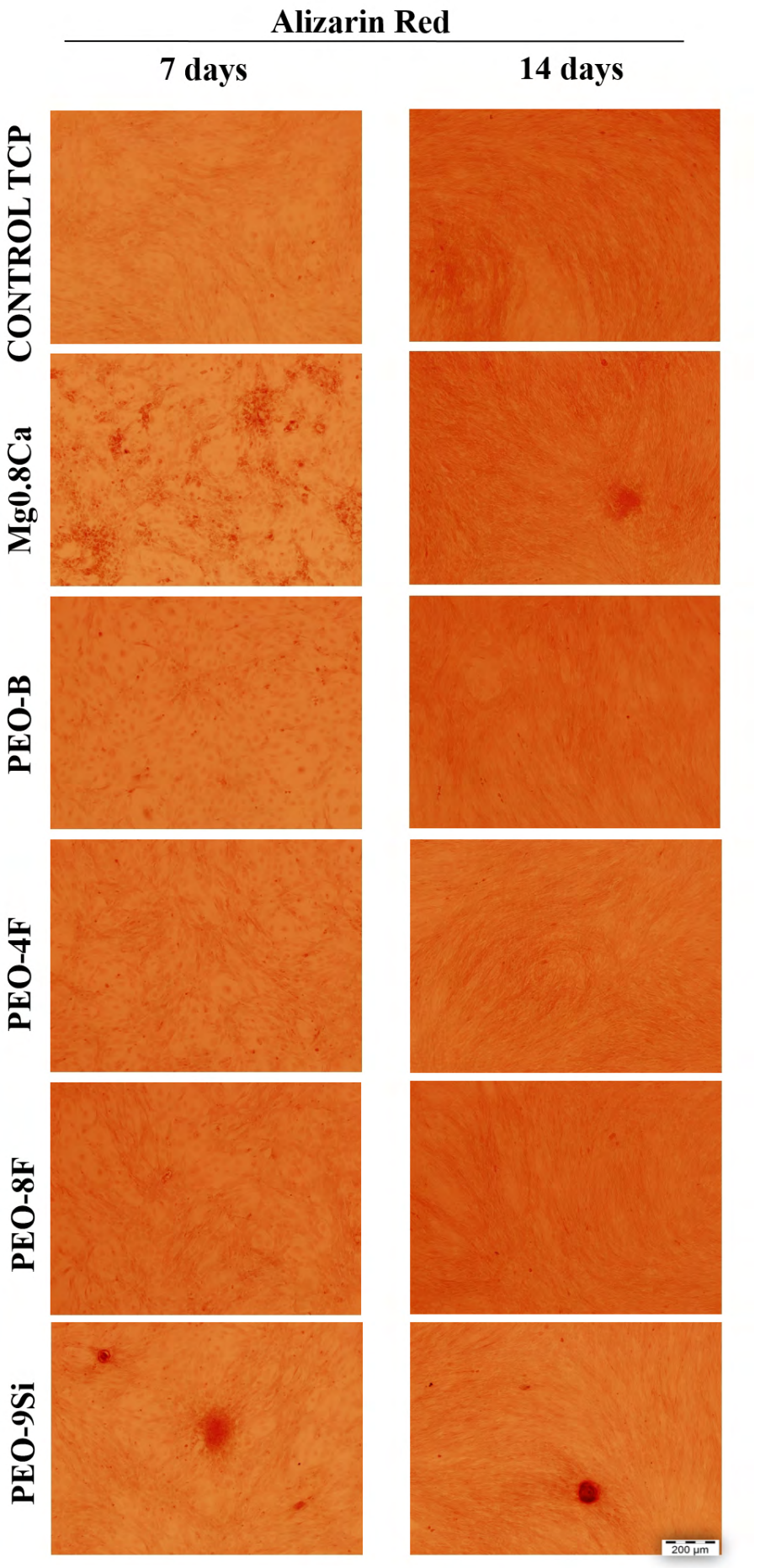
Alizarin Red
7 days
14 days
CONTROL TCP
Mg0.8Ca
PEO-B
PEO-4F
PEO-8F
PEO-9Si
200 µm

CONTROL TCP

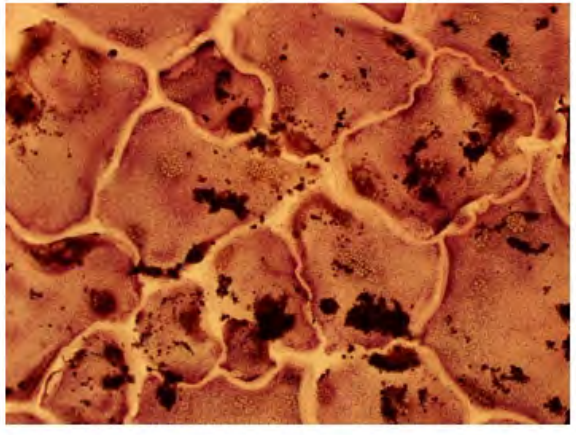

Mg0.8Ca

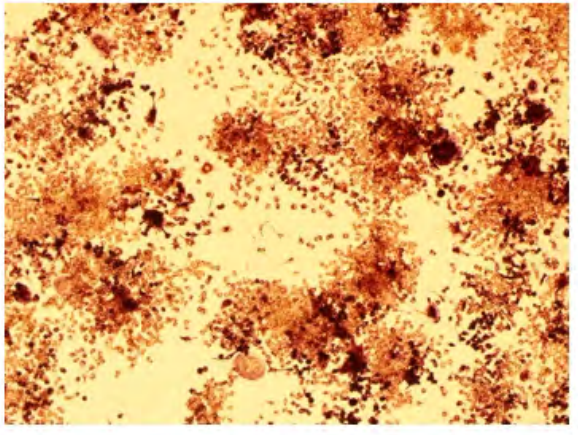

PEO-B

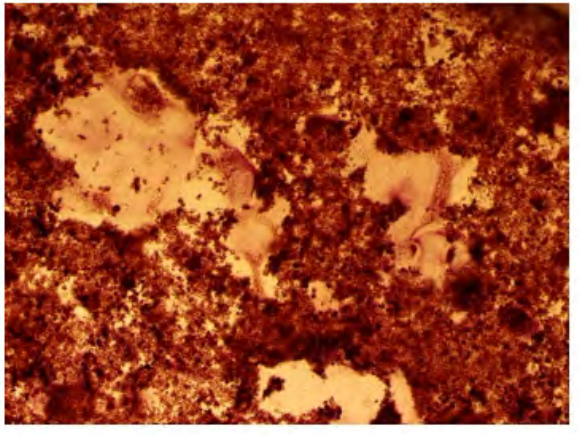

PEO-4F

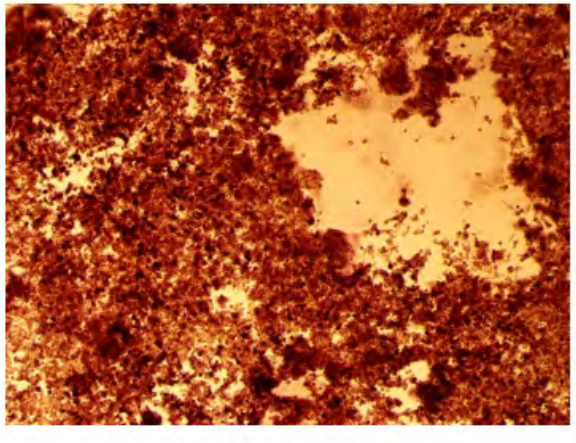

PEO-8F

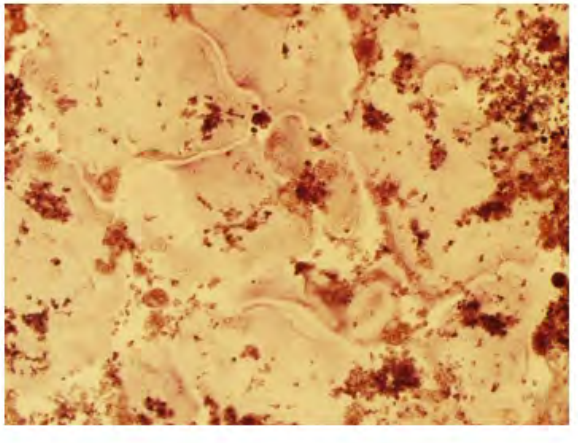

PEO-9Si

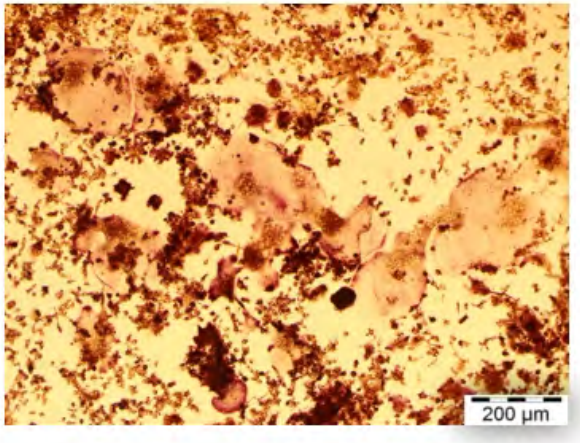

ACTIN
HOECHST
TRAP
CONTROL TCP
Mg0.8Ca
PEO-B
PEO-4F
PEO-8F
PEO-9Si
200 µm

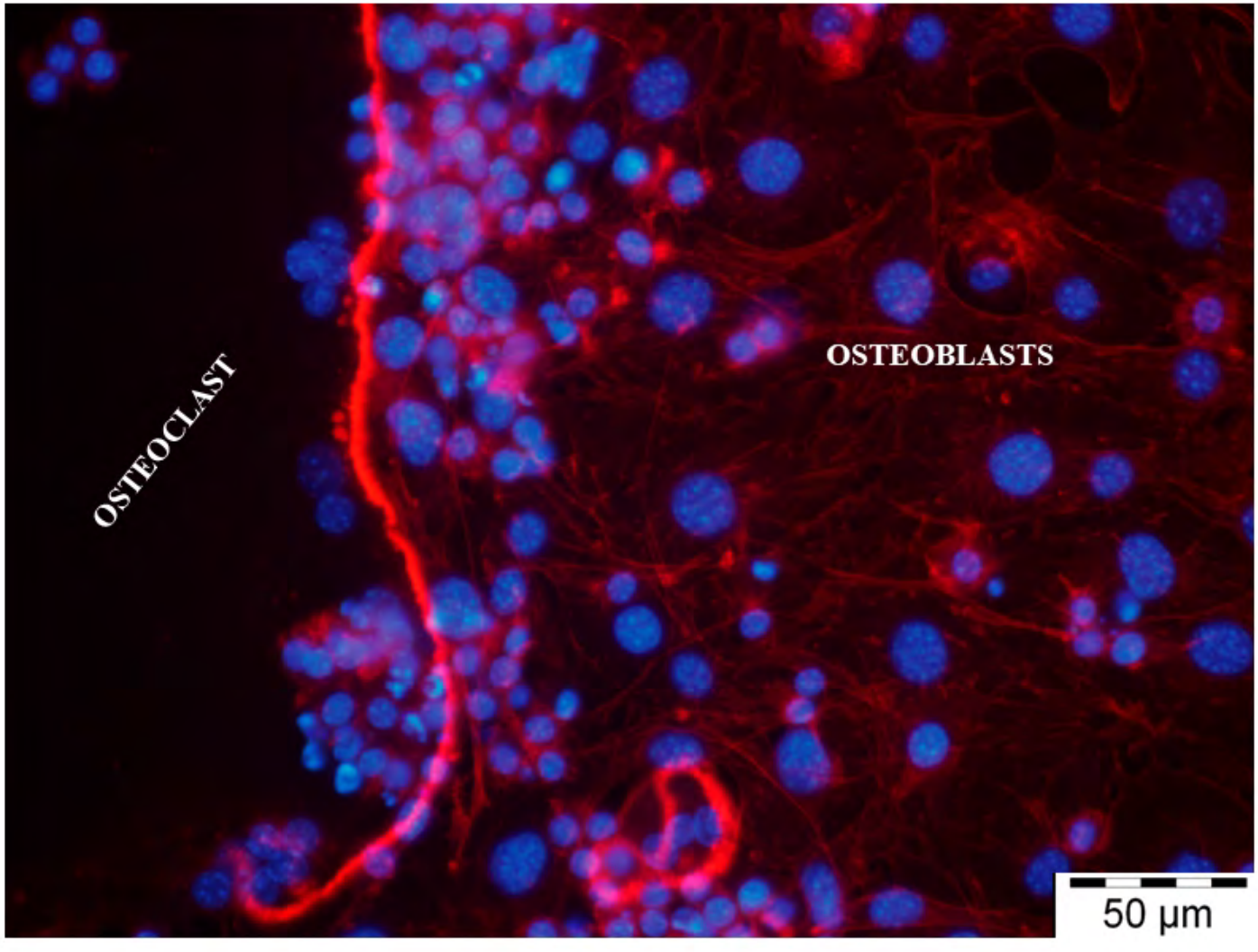
OSTEOCLAST
OSTEOBLASTS
50 µm

Electrolyte components	***PEO-B***	***PEO-4F***	***PEO-8F***	***PEO-9Si***
	g L^{-1}	g L^{-1}	g L^{-1}	g L^{-1}
KOH	1	1	1	1
$Na_3PO_4 \cdot 12H_2O$	10	10	10	10
CaO	2.9	2.9	2.9	2.9
NaF	-	4	8	-
$Na_2SiO_3 \cdot 5H_2O$	-	-	-	9
pH	12.7	12.4	12.5	12.9
σ *mScm*$^{-1}$	13.9	23.5	30.2	22.7

Coating / Location		*Elements*							*Ratios*
		Mg	**O**	**P**	**Ca**	**F**	**Na**	**Si**	***Ca/P***
PEO-B	**1**	48.8	44.7	3.3	2.1	-	1.2	-	0.66
	2	53.	42.1	3.1	0.5	-	0.6	-	0.14
PEO-4F	**3**	22	50.2	7.1	9.1	8.6	2.8	-	1.32
	4	32.6	33.3	12	15.5	4.6	2	-	1.29
	5	54.7	15.7	5.5	0.03	24.1	0.1	-	0.01
PEO-8F	**6**	25.8	42.5	6.6	10.2	11.1	3.7	-	1.55
	7	33.7	33	8.8	12.4	8	4.1	-	1.41
	8	42.6	11.3	6.3	0.2	39.2	-	-	0.02
PEO-9Si	**9**	36.5	48	2.5	1.1	-	1.8	10.1	0.45
	10	41.1	42	3.3	0.5	-	1	12.1	0.16
	11	64.5	25.4	0.6	2.2	-	0.4	7	3.79

Coatings		***PEO-B***	***PEO-4F***	***PEO-8F***	***PEO-9Si***
Roughness (μm)	R_a	0.7 ± 0.02	4.3 ± 0.3	3.6 ± 0.3	0.84± 0.01
	R_z	4.7 ± 0.2	24.2 ± 1.7	22.9 ± 1.9	5.6 ± 0.3
Surface Porosity (μm^2)	*Max.*	*	*	*	4.50
	Min.	*	*	*	~0.3
Transversal Porosity (μm^2)	*Max.*	*	115.4	29.5	*
	Min.	*	~0.9	~0.9	*
Surface pore population density ($pores/mm^2$)		*	*	*	1705
Thickness (µm)		6.4 ± 0.7	47.5 ± 2.7	48.6 ± 4.0	12.7 ± 1.3
Microhardness (HV)		***	182 ± 40	360 ± 80	240 ± 60

* Not evaluated due to limitations of image analysis

** Not evaluated due to the technique limitation (too thin coating)

Samples	*Elements (μg cm^{-2} d^{-1}, ppm*)*							
	Mg		**Ca**		**P**		**Si**	
PEO-B	46.1 ± 4.4	42±4	2.0 ± 0.2	1.8±0.2	0.7 ± 0.1	0.6±0.1	-	
PEO-4F	354.6 ± 35.1	323±32	11.4 ± 1.1	10.4±1.0	4.2 ± 0.4	3.8±0.4	-	
PEO-8F	305.2 ± 30.7	278±28	15.9 ± 1.6	14.5±1.5	3.8 ± 0.4	3.5±0.4	-	
PEO-9Si	70.3 ± 6.6	3.5±0.4	1.1 ± 0.1	1.0±0.1	1.1 ± 0.1	1.0±0.1	2.2 ± 0.2	2.0±0.2
Mg 0.8 Ca	65-417	59-382	5.2 ± 4.6	8.5±0.4	-		-	

* ppm values are provided for 5 days of immersion.

Conditions	*F (μg cm^{-2}, ppm)*			
	1 day		**5 days**	
PEO-4F	63.7 ± 1.0	11.8±0.2	12.7 ± 0.2	2.3±0.1
PEO-8F	118.9 ± 8.5	22.0±1.6	7.0 ± 0.5	1.3±0.1

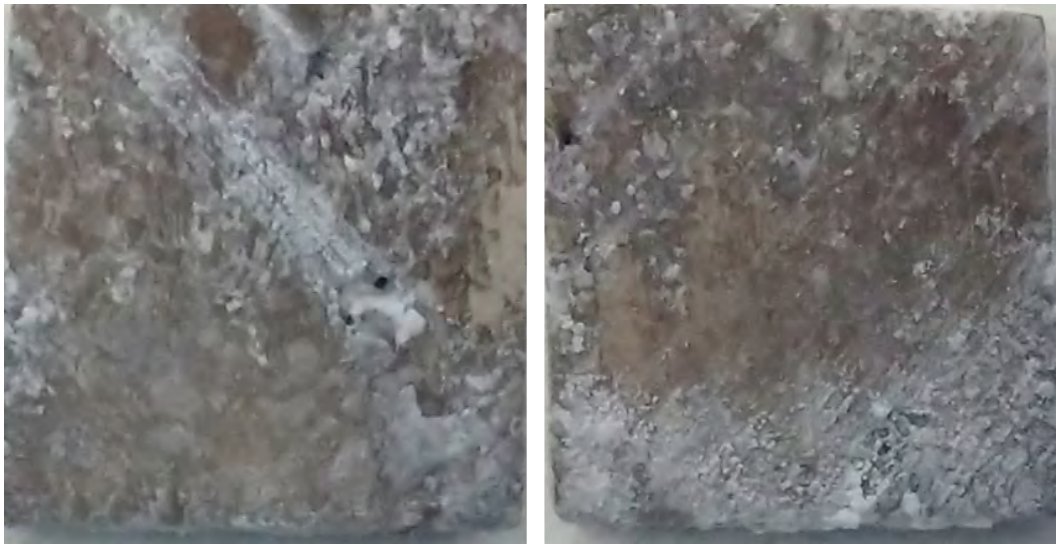

Supplementary Figure 1. Mg0.8Ca alloy (1×1 cm^2) after 5 days of immersion in 0.9% NaCl.

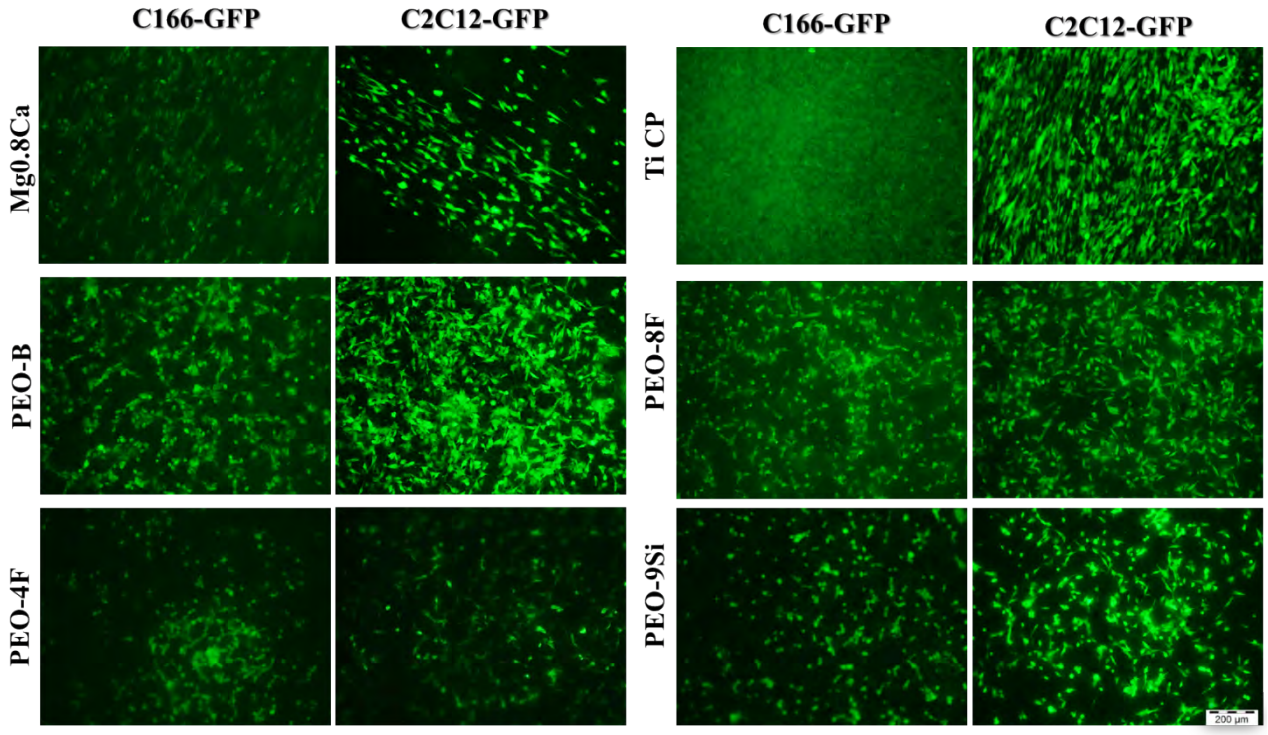

Supplementary Figure 2. Endothelial C166-GFP and premyoblastic C2C12-GFP cells growing over the bare alloy (Mg0.8Ca), control Ti CP and the ceramic coatings (PEO-B, PEO-4F, PEO-8F and PEO-9Si) after 24 h of seeding.

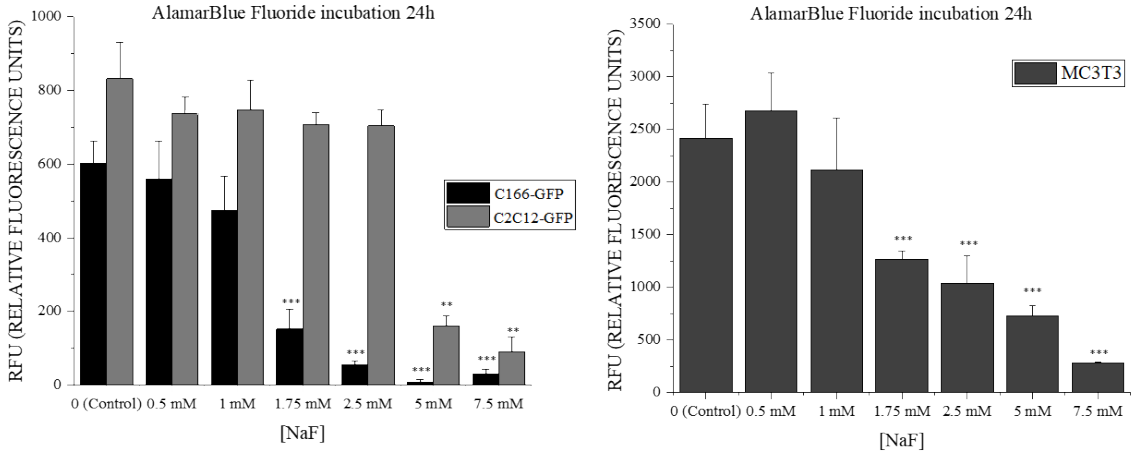

Supplementary Figure 3. NaF cytotoxicity study with C166-GFP, C2C12-GFP and MC3T3 cell lines.

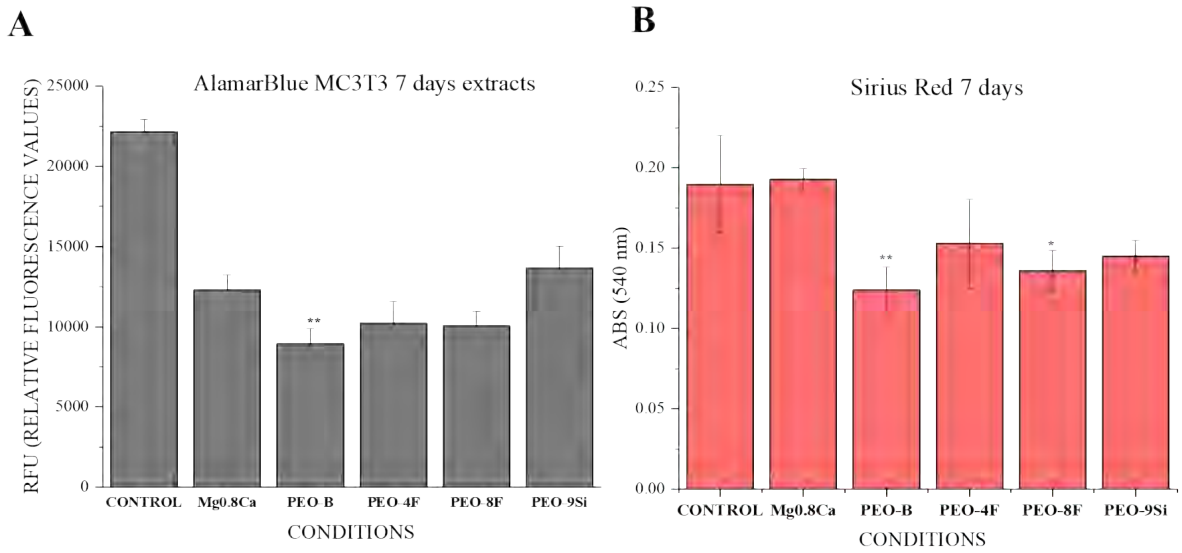

Supplementary Figure 4. A. Metabolic activity evaluation of MC3T3 cells after 7 days growing in contact with 1:4 extracts. **B.** Sirius Red quantification at day 7 of culture.